Microwave Spectroscopic Study of Methyl Salicylate and Water Clusters

by

Supriya Ghosh

A thesis submitted in partial fulfilment of the requirements for the degree of

Master of Science

Department of Chemistry

University of Alberta

Abstract

Details about different types of hydrogen bonding, for example strong and weak, conventional and unconventional, will be discussed. Similarly the significance of H-bonding in different fields of science will also be discussed along with theoretical descriptions. A brief description about two spectrometers, namely a cavity-based and a chirped-pulse Fourier transform spectrometer are given. These spectrometers were used to measure the high resolution microwave spectra of the methyl salicylate monomer and its clusters with water produced in a supersonic jet expansion. The mechanism for the experimentally observed dual fluorescence of methyl salicylate (MS) is a long standing research topic. Two distinctively different H-bonded methyl salicylate-water conformers, one with carbonyl O and the other with hydroxy O serving as the hydrogen-bond acceptor, were detected using chirped pulse and cavity based Fourier transform microwave spectroscopy and found to be of comparable stability. This observation provides direct experimental evidence for the previously undetected hydroxy O-bonded conformer, supporting the recently proposed new mechanism for the dual fluorescence of MS in protic solvents. An interesting interplay between the methyl internal rotation and water tunneling motions was also investigated. The existence of an unconventional O···H-C hydrogen-bond was verified using the atoms-in-molecules theory. Thorough searches for the elusive ketoA, a high energy conformer of MS, were conducted. My results support the recent theoretical reports that only one MS conformer exists in the ground state.

Preface

This thesis is based on the research I have done at the University of Alberta between September 2012 and July 2015. Chapter 3 of this thesis has been reproduced in part from the following publication: Ghosh, S.; Thomas, J.; Huang, W.; Xu, Y.; Jäger, W. "Rotational Spectra of Two Hydrogen-Bonded Methyl Salicylate Monohydrates: Relative Stability and Tunneling Motions", J. Phys. Chem. Lett. **6**, 3126 (2015).

Dedicated to my parents

Acknowledgement

I would like to thank to several people who have provided me with guidance and support during my M.Sc studies. First and foremost, I would like to express my sincere gratitude to my supervisor Prof. Wolfgang Jäger for the continuous support in my research. I am very grateful for the considerable latitude and independence he has given me during my studies.

I also want to thank Prof. Yunjie Xu for her support and helpful discussions during my M.Sc study. I am also thankful to Prof. Alex Brown for his support and assistance.

I am also grateful to all those people in the Machine and Electronic shop. I am also thankful to my teaching assistant coordinators Dr. Norman Gee and Dr. Anna Jordon for their support. My sincere thanks also go to the Jäger and Xu group members Javix, Nathan, Prasanta, Elijah, Chrissy, Amin, Angelo, Joseph, Jiao, Wenyuan, Dan, Xiaoli.

I would also like to thank to all my friends for their support and suggestions during these three years. I owe special thanks to my parents, my sister and my brother for their love and unconditional support.

Table of Contents

LIST OF TABLES

List of Figures

LIST OF SYMBOLS

ρ	Electron density
$\hat{H}$	Hamiltonian operator
Ψ	Time independent wave function
C_p	Specific heat at constant pressure
C_v	Specific heat at constant volume
K	Boltzmann constant
γ	Heat capacity ratio
Ψ_f	Final state wave function
Ψ_i	Initial state wave function
$\hat{\mu}_g$	Dipole moment operator
J	Rotational level
$E_{rot}(J)$	Rotational energy
$\widehat{H}_0$	Time independent Hamiltonian operator
$\hat{I}$	Moment of inertia
$Y_J^M(\theta, \phi)$	Spherical harmonics
$P_J^{\lvert M \rvert}$	Associated Legendre polynomial
N_{JM}	Normalization constant
$J_{K_a K_C}$	Rotational level
μ_a, μ_b, μ_c	Dipole moment components
A, B, C	Rotational constants
T_2	Macroscopic polarization decays rate
ω_R	Rabi frequency
$\mu_{f \leftarrow i}$	Electric dipole moment of the transition between levels i and f

Q	Quality factor of the cavity
ν_{MW}	microwave frequency
$\Delta\nu_m$	Offset frequency

LIST OF ABBREVIATIONS

HF	Hartree Fock method
MP2	Møller Plesset perturbation theory of second order
DFT	Density functional theory
BSSE	Basis set superposition error
CP	Counterpoise correction scheme
FTMW	Fourier Transform microwave spectrometer
c.o.m	Center of mass
PIN	p.i.n diode
A/D	analog-to-digital converter
AWG	arbitrary waveform generator
TTL	transistor-transistor logic
RF	radio frequency
CP-FTMW	Chirped pulse Fourier transform microwave spectrometer
PDRO	phase-locked dielectric resonator oscillator
MS	Methyl salicylate
SOA	Secondary organic aerosols
VOC	Volatile organic species
CCN	Cloud condensation nuclei
UV	Ultraviolet
ESIPT	Excited state *intra*molecular proton transfer
IR	Infrared

Chapter 1

Introduction

1.1 Hydrogen Bonding

1.1.1 Intermolecular Interactions

Intermolecular interactions are omnipresent and govern, for example, structures of organic, organometallic, and biomolecules, crystal packing, drug-receptor interactions, and also selectivity of chemical reactions. They also play important roles in determining physical properties of substances, such as vapour pressure, melting point, boiling point, viscosity, surface tension, solubility, etc. Neglecting interactions involving ions, intermolecular forces can be classified into four types: Keesom forces, which result from interactions between permanent electric multipole moments, Debye forces, which are due to interactions between permanent and induced multipole moments, London dispersion forces (induced multipole-induced multipole interactions), and hydrogen bonding.

Among the different types of intermolecular interactions, hydrogen bonding has probably attracted the most interest because of its great significance in chemistry, biology, and also in physics.[1] According to Pauli[2] "under certain conditions an atom of hydrogen is attracted by rather strong forces to two atoms, instead of only one, so that it may be considered to be acting as a bond between them. This is called the hydrogen bond." The hydrogen bond, or short H-bond, is a noncovalent interaction between a proton donor (X-H) and a proton acceptor (Y), which is generally weaker than a typical covalent bond. In a conventional H-bond, the X and Y atoms have a higher electronegativity than hydrogen, such as, for example O, F, Cl, and S. The electronegative X atom attracts the electrons in the X-H bond, and creates a partial positive charge on the hydrogen atom. This hydrogen atom is in turn attracted by the lone pair of the electronegative Y atom. For weak H-bonds, the interaction is mainly electrostatic in nature, but for strong H-bonds dispersion effects can play important roles. The H-bond can be present in both gaseous, liquid, and even in solid phases. It can be both *inter*molecular (X and Y belong to different molecules) or *intra*-molecular (X and Y belong to the same molecule). In the case of intramolecular H-bonding it is often a bent bond, whereas the intermolecular H-bond is generally linear or close to linear. Depending on the strength, H- bonding can be weak, moderate, and also as strong as a covalent bond. The strength of moderate (conventional) H-bonding interaction ranges from 4 to 15 kcal/mol. Weak H-bonding interactions are in the range of 2-4 kcal/mol, and are similar in magnitude as London dispersion forces, whereas strong H-bonding interactions are in the range of 15-40 kcal/mol, in the same range as covalent bonds. Similarly, the bond distance of an H-bond

(H...Y) can be > 2 Å for weak H-bonds and between 1.2 and 1.5 Å for a strong H-bond.[1,3] The strength of the H-bond also depends on the X-H…Y angle. For strong H-bonding the angle is between 170 ° and 180 ° (linear or nearly linear), whereas the angles for weak H-bonds are generally between 90° and 180°. H-bonding is not a simple interaction; it has contributions from dispersion, electrostatic, and covalent interactions, and also from polarization effects.[4]

Experimental evidence for the presence of H-bonds can be found in terms of a particular change of molecular geometry or some other physical or chemical property. For example, if H-bonding occurs, the X-H bond will become longer than its usual bond length. At the same time, the H···Y distances become shorter than the sum of van der Waals distances of those atoms. In conventional H-bonding, the frequencies of the X-H and Y-Z (Y-Z could for example be a O=C bond) stretching modes are red shifted with respect to the free, non H-bonded case. The effect of H-bonding can also be seen in NMR studies.[5] The proton which is involved in the H-bond, experiences deshielding, causes a chemical shift to lower field.

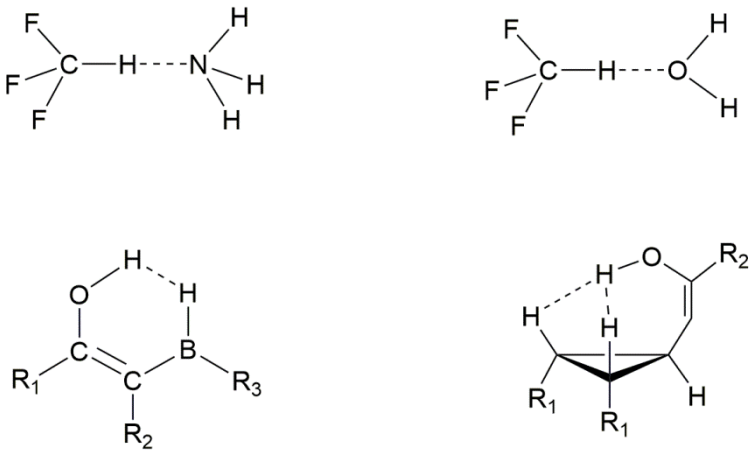

Figure 1.1 Examples of unconventional H-bonds.[4]

Other than the "conventional" or "classical" H-bond, there are examples of "unconventional" H-bonds, where the natures of the H-bond donors and acceptors are different from those of conventional donors and acceptors. Cases of unconventional H-bonding can be grouped into three types: those with an unconventional donor, those with an unconventional acceptor, and those with both unconventional donor and acceptor. An example of the first type would be a C-H bond that can act as a proton donor. The fact that a C-H group can act as an H-bond donor was first proposed by Sutor in the early 1960s.[6, 7] Later on, studies have shown that the C-H group can indeed act as a H-bond donor in many systems, such as amino acids,[8]

nucleic acids,[9-11] and other biomolecules.[12] An example for the second kind is one where a π-electron system acts as an acceptor. Both theory and experiment have shown that π-electron clouds can act as an H-bond acceptor in a variety of systems.[13,14] An example of the third kind is a dihydrogen bond, where a protic X-H group and a hydridic H-Y group are involved. This type of H-bond occurs between two H atoms, where one H atom accepts an electron from the other H atom ($X^{\delta-}$-$H^{\delta+}\cdots\cdots H^{\delta-}$-$Y^{\delta+}$).[15-17]

In a further type of unconventional H-bond, a metal atom can act as an acceptor. Though direct involvement of a metal atom in H-bonding seems unusual, there is good evidence for the formation of such H-bond. In a recent paper[18], Ogasawara *et al*. have shown the formation of an H-bond involving a water molecule on a Pt metal surface during the adsorption of water. They could demonstrate, with the help of x-ray photoelectron spectroscopy and DFT calculations, that water molecules in the first layer bind directly to the surface of Pt through H bonding. There is also evidence for a metal acting as an H-bond donor (X). In their paper,[19] Epstein *et al.* have shown that when $(\eta^5\text{-}C_5Me_5)_2$ and PPh_3O are combined in a CH_2Cl_2 solution, an Os-H$\cdots$O(=P) hydrogen onded adduct results. This was proven by IR studies of the Os-H and P=O stretching vibrations and comparison to the isolated $(\eta^5\text{-}C_5Me_5)_2$ and PPh_3O molecules.

1.1.2 Importance of Hydrogen Bonding

H-bonding can be responsible for physical properties (such as melting point, boiling point, density etc.) for many substances. For example H_2O, HF and NH_3 have higher boiling points than the compounds formed between hydrogen and the corresponding next group elements, i.e. H_2S, HCl, and PH_3. The H-bond also affects the melting point of substances. For example *o*-nitrophenol has a lower melting point than *p*-nitrophenol. This is because *p*-nitrophenol forms intermolecular H-bonds, whereas *o*-nitrophenol has an *intra*molecular H-bond. As a result, it is easy to separate these molecules from each other. Viscosity is another physical property that can depend on H-bonding. Molecules that can form *inter*molecular H-bonds are more viscous than those without H-bonding. The density of substances can also be affected by H-bonding. For example, at 4 °C the density of water is a maximum. Other physical properties, such as heat capacity, color, dielectric constant, dipole moment, heats of mixing and dilution also depend sometimes on the H-bonding interactions present in the system.

H-bonding interactions play also important roles in determining structure and function of biomolecules. The H-bonding interactions present in the base pairs of nucleic acids have an important role in the double helical structure of DNA and RNA.[20] Nucleotides present in DNA and RNA form pairs via H-bonding.[21] For example, thymine has one H-bond donor and one H-bond acceptor site which perfectly pairs with the complementary adenine. Similarly, guanine pairs with cytosine via three H-bonding sites. Numerous experimental and theoretical studies have been done on hydration of DNA.[22,23] It was shown that nucleic acids have three levels of hydration shells and that the conformation of DNA is very sensitive to hydration. [25] The primary hydration shell involves about 12 water molecules and is impermeable to cations. The secondary hydration shell is permeable to cations and the third shell is completely disordered. H-bonding also affects protein structure, protein folding, and enzyme catalysis. H-bonding is important in determining secondary structures of proteins, such as α-helices, β-sheets, and π-helices.[21, 24] The biological activity of proteins also depends on the dynamic equilibrium of making and breaking of H-bonds.[25] Several studies have also been done on the solvation dynamics of proteins to gain knowledge about the protein folding process and enzyme action.[26] Antibodies are three dimensional folded protein structures that target a specific antigen in a lock and key fashion. The antibody interacts with the antigen through a number of weak interactions including H-bonding.

1.1.3 Theoretical Calculations of H-bonds

Initially it was thought that H bonding is purely electrostatic in nature. Pauling[27] also wrote that an H-atom can only form one covalent bond, so that the second bond (i.e. the H-bond) must be the result of an ionic interaction between a (partially) positively charged hydrogen and a (partially) negatively charged acceptor. A number of workers have carried out H-bond calculations using a simple electrostatic model.[28,29] Though this model could explain certain aspects of the H-bond, such as the shift in the X-H force constant[30] in the H-bonded systems, there were strong arguments against the exclusive electrostatic model[31]; firstly, changes in intensity in the infrared spectra upon H-bond formation prove that there must be a charge redistribution upon bond formation; secondly, there should be a considerable amount of repulsion between the two fragments at the H-bond distance. This repulsion energy actually nullifies the good agreement between the H-bond energy calculated from the simple electrostatic model and the experimental H-bond energy.

To include those contributions in H-bonding, Coulson[32] *et al.* and Tsubomura[33] have introduced an empirical valence bond approach. Though the qualitative valence bond approach was very important to rationalize many important phenomena relating to H-bonding, especially at a time when non-empirical methods could not be carried out, no quantitative results could be obtained from those calculations. This approach also failed to explain some basic aspects, such as, for example, why some H-bonds are stronger than others.

Previously, a number of molecular orbital studies have been done on H-bonded systems using different models. In 1958 Hofacker[34] used a localized orbital method, where the MOs of the complex were expressed in terms of the MOs of the fragments and perturbation terms. In 1958, a three-center four-electron MO wave function was used by Paolini[35] to represent an H-bond and he concluded that the p-orbital on the H-atom also takes part in H-bonding, though later studies proved that it has only little effect[36]. Later, calculations using valence bond and MO methods have also been carried out by Bessis and Bratoz[37] and Erdahl[38], where the nonrelativistic Schrödinger equation was solved using a non-orthogonal atomic basis in a multideterminant wave function. Though it gave reasonable results for small systems, this method was difficult to apply to larger systems. Some of the many other MO studies were very important at a time when fast computers were not available.

A variety of quantum mechanical models are currently used to analyse H-bonding. Among them, semi-empirical MO methods, Hartree-Fock (HF), post-HF, and density functional theory (DFT) based methods are widely used. The exchange term present in HF calculations makes this method very useful as it considers the electrostatic contribution in H-bonding. Post-HF methods, such as Møller-Plesset (MP) (e.g. MP2, MP4) and coupled-cluster (CC) methods (e.g. CCSD) are widely used because they include electron correlation and account for intermolecular electron dispersion interactions. Alternatively, the DFT method (such as B3LYP) was also found to be very useful for H-bonding studies, though it does not consider electron correlation systematically. Various properties affected by H-bonding, such as bond lengths, bond angles, interaction energies, and vibrational spectra are influenced by the basis sets used in the calculation. Hence different combinations of methods and basis sets are often used to obtain good estimates for the interaction energy and other parameters. Details about *ab initio* calculations and basis sets used to model H bonds adequately are given in Chapter 2.

Bader's "Atoms in molecules" (AIM) theory is often applied to analyse H-bond interactions in various *inter*molecular and *intra*molecular systems.[39] This theory allows studying the strength of a chemical bond by using the electron density. According to this theory, the electron density, ρ, near the atom changes during bond formation. In particular, there is a bond critical point (the point where the gradient of ρ between two bound atoms has a minimum) that characterizes a chemical bond. Numerous studies have been done to characterise both strong or weak and conventional or unconventional H-bonding using the AIM theory.[40,41]

Though quantum calculations are very useful to estimate H-bond strengths and other properties related to H-bonding, this approach is not feasible for larger systems, such as DNA, proteins, and DNA-protein complexes. For those type of systems, molecular mechanics (MM) and molecular dynamics (MD) approaches are found to be very useful methods to study the structures and dynamics.

1.1.4 Microwave Studies of H-bonded Systems

Rotational spectroscopy is one of the most important experimental methods which can provide detailed structural information of molecular complexes, including those with H-bonds. From the measured rotational transition frequencies, rotational constants can be determined, which, in turn, can be used to derive structural parameters. Although rotational spectra of some hydrogen bonded complexes were measured using a static gas sample and the method of Stark spectroscopy,[42] low number densities of the complexes and rather low spectral resolution limited the applicability of these methods to the study of H-bonded clusters.

Molecular complexes can be formed very effectively when molecules are expanded into a vacuum chamber by supersonic jet expansion. Numerous studies have been done to determine the structure of molecular complexes formed by a supersonic jet expansion using microwave spectroscopy. The first rotational transitions in supersonic beams were studied by Dyke *et al.* for the complexes $(HF)_2$ and Ar-HCl using electric resonance molecular beam spectroscopy.[43] Later on, Balle and Flygare[44] developed pulsed-nozzle Fourier transform microwave spectroscopy. Details about this type of spectroscopy are given in Chapter 2. A Fourier transform microwave spectrometer provides high spectral resolution, and as a result

splittings which result from, for example, *intra*molecular tunneling motions and coupling between nuclear spins with rotational angular momentum, can be measured and analyzed.

The more recently developed method of chirped pulse Fourier transform microwave spectroscopy allows one to measure broadband rotational spectra of molecular clusters.[45] Details about this type of spectrometer are given in Chapter 2.

1.2 Methyl Salicylate (Oil of Wintergreen)

1.2.1 Natural Occurrence and Synthesis

Methyl salicylate (MS) is a naturally occurring organic ester produced by a number of different plants. Many plants produce MS in small amounts, but several species produce more significant amounts. These species include *Gaultheria Procumbens* (wintergreen or eastern teaberry) of the genus *Gaultheria*, *Betula Lenta* (black birch or cherry birch) of the genus *Betula*, and all species of the genus *Spiraea*. Steam distillation of twigs of sweet birch and eastern teaberry gives MS and people have used this method in the past to produce MS. "Oil of wintergreen" contains about 98% MS. Commercially, MS is synthesised by esterification of salicylic acid and methanol.

1.2.2 Significance of Methyl salicylate

a) Messenger Molecule for Plants

Methyl salicylate is an example of green leaf volatile compound (GLV) which is emitted by some plants in stress conditions. For example, if such a plant is affected by herbivorous insects, experiences drought, heat, or cold, it releases MS.[46,47] The MS can be detected by other parts of the same plant, other plants of the same species, or even plants of different species, which respond by mobilizing their immune system. For example, when tobacco plants are affected by the tobacco mosaic virus, the plant emits MS which act as an aid by killing the virus and it also warns the other plants about the pathogen by airborne signaling and activates the plant's immune system.

b) Medical Uses and Side Effects

Methyl salicylate is an ingredient in some ointments used as a topical analgesic to relieve minor aches and pain caused by arthritis, sprains and strains (e.g. Ben Gay®, Icy Hot®). Although it is widely used as a popular pain relieving cream, a report shows that one

teaspoon of MS has the same toxicity as 21 tablets of aspirin; an overdose of MS can have severe side effects.

c) Atmospheric Significance

Methyl salicylate is present at low concentration in atmosphere. It is very interesting for its importance to the atmosphere and climate. Secondary organic aerosols are one of the important species in the atmosphere that have impact on climate, atmospheric processes, cloud formation and human health. SOA is formed when volatile organic species react with atmospheric oxidants (such as reactive oxygen species, ozone or OH radical). Methyl salicylate being a VOC also acts as a precursor for SOA.[48] It is found that under foggy conditions, methyl salicylate forms SOA via aqueous reactions with OH radical.[49]

d) Spectroscopic Importance

Weller discovered in 1966 that MS exhibits a dual fluorescence spectrum, with a blue band around 440 nm and a UV band around 360 nm.[50] To explain this observation, Weller proposed the existence of a double well potential in the electronically excited state. Upon excitation, MS undergoes an *intra*molecular proton transfer to reach the second well, from which the UV fluorescence occurs. Weller's proposed photophysical scheme was the foundation of what is known as "excited state *intra*molecular proton transfer" (ESIPT). Since then, many studies have been done to explain the simultaneous dual fluorescence emission spectrum of MS. Theoretical studies suggest that the proton transfer in the excited state is barrier-less, such that the double well cannot explain the dual fluorescence.[51-55] Very recently, a promising proposal was made, which relates the dual fluorescence to two different solvent – MS conformers in the ground state.[56]

1.3 Outline of This Study

This thesis is divided into four chapters, the first being the introduction. The second chapter consists of mainly two parts; a theoretical and an experimental section. In the theoretical part, I give some background about ab initio calculations and discuss different levels of theory and the significance of basis sets with regard to geometry optimizations and energy calculations is discussed. In the experimental part, I describe some basics of microwave spectroscopy, and give an overview of our cavity-based and chirped-pulse Fourier transform microwave spectrometers, along with a brief description of their operating

principles. In this section, I also describe how to simulate and interpret the experimental rotational spectra using several computer programs for spectral analyses.

In Chapter 3, I describe the main focus of this study i.e. the study of methyl salicylate and its complex with water using ab initio calculations and microwave spectroscopy. This includes previous work related to this research, my ab initio calculations to predict the different conformers, experimental proof of the conformers, rotational constants, splittings of rotational transitions due to methyl group internal rotation and water tunneling, and an interpretation of the findings. Finally a brief conclusion and possible future work are described in chapter 4.

[1] Jeffrey, G. A.; Saenger, W. Hydrogen Bonding in Biology and Chemistry (Springer-Verlag, Berlin, 1991).

[2] Pauling, L. The Nature of the Chemical Bond (Cornell University press, Ithaka, New York, 1960).

[3] Jeffrey, G. A. An Introduction to Hydrogen Bonding (Oxford University Press, New York, 1997).

[4] Grabowski, S. J. Hydrogen Bonding – New Insights (Springer, New York, 2006).

[5] Berglund, B.; Vaugham, R.W. *J. Chem. Phys.* **1980**, 73, 2037-2043.

[6] Sutor, D.J. Nature **1962**, 195, 68-69.

[7] Sutor, D.J.; *J. Chem. Soc*. **1963**, 1105-110.

[8] Ramachandran, G.N.; Chandrasekharan, R. Biopolymers **1968**, 6, 1649-1658.

[9] Sussman, J.L.; Seeman, N.C.; Kim, S.-H.; Berman, H.M. *J. Mol. Biol*. **1972,** 66, 403-421.

[10] Rubin, J.; Brennan, T.; Sundaralingam, M. *Biochem.* **1972**, 11, 3112- 3128.

[11] Saenger, W. *Angew. Chem., Int. Ed. Engl.* **1973,** 12, 591-601.

[12] Kvick, A.; Koetzle, T. F.; Thomas, R. *J. Chem. Phys.* **1974**, 61, 2711- 2719.

[13] Desiraju G. R.; Steiner, T. The Weak Hydrogen Bond in Structural Chemistry and Biology (Oxford University Press, Oxford, 1999).

[14] Saggu, M.; Levinson N. M.; Boxer S. G. *J. Am. Chem. Soc.* **2012**, 134, 18986-18997.

[15] Grabowski, S.J. *Chem. Phys. Lett*. **1999**, 312, 542-547.

[16] Palusiak, M.; Grabowski, S. J. *J. Mol. Struct. Theochem*, **2004**, 674, 147-152.

[17] Grabowski, S. J. *J. Phys. Chem. A*, **2000**, 104, 5551-5557.

[18] Ogasawara, H.; Brena, B.; Nordland, D.; Nyberg, M.; Pelmenschikov, A.; Petterson L. G. M.; Nilsson, A. *Phys. Rev. Lett.* **2002**, 89, 276102(1-4).

[19] Epstein, L. M.; Shubina, E. S.; Krylov, A. N.; Kreindlin A. Z.; Ribinskaya, M. I. *J. Organomet. Chem.,* **1993**, 447, 277-280.

[20] Schulz, G. E.; Schirmer, R. H. Principles of Protein Structure (Springer- Verlag, New York, 1979)

[21] Sponer, J.; Leszczynski, J.; Hobza, P. *J. Phys. Chem.* **1996**, 100, 1965-1974.

[22] Leszczynski, J.; *Adv. Mol. Struct. Res*. **2000**, 6, 209-265.

[23] Saenger, W. Principles of Nucleic Acid Structure (Springer-Verlag, New York, 1984).

[24] Lehninger, A. L.; Nelson, D. L.; Cox, M. M. Lehninger Principles of Biochemistry (Worth Publishers, New York, 2000).

[25] Fersht, W. H. A. Structure and Mechanism in Protein Science: A Guide to Enzyme Catalysis and Protein Folding (W. H. Freeman and Company, New York, 1999).

[26] Wong, M. A.; Frisch, M. J.; Wiberg, K. B. *J. Am. Chem. Soc.* **1992**, 114 , 523- 529.

[27] L. Pauling, *Proc. Nat. Acad. Sci.* **1928**, 14**,** 359.

[28] Pimentel G. C.; McClellan, A**.** L. The Hydrogen Bond (W.H Freeman, San Francisco Calif., 1960)

[29] Hamilton, W. C.; Ibers, J. Hydrogen Bonding in Solids (W**.** A. Benjamin, New York, N. Y., 1968).

[30] Bader, R. F. W. *Can. J. Chem.,* **1964**, 42,1822-1834.

[31] Kollman P.A.; L.C. Allen, *Chem. Rev*. **1972,** 72, 283-303.

[32] Coulson C. A.; Danielson, U. *Ark. Fys*.**, 1955,** 8*,205*- 239.

[33] Tsubomura, H. *Bull. Chem.Soc. Jap.* **1954**, 27,445.

[34] Hofacker, L.; *Z. Naturforsch. A,* **1958**, 13, 1044.

[35] Paolini, L. *J. Chem. Phys.* **1959***,* 30, 1045.

[36] Kollman, P. A.; Allen, L. C. *J. Am. Chem. Soc.* **1970**, 92, 4108-4110.

[37] Bessis G.; Bratoz, S**.** *J. Chim. Phys.* **1960**, 57, 769.; Bessis, G. *Can. Phys.* **1961**, 127, 105.

[38] Erdahl, R. M. Ph.D. Thesis, Princeton University, 1965.

[39] Bader, R. F. W. *J. Phys. Chem. A* **1998**, 102, 7314−7323.

[40] Popelier, P. L. A. *J. Phys. Chem*. A**, 1998**, 102, 1873-1878.

[41] Alkorta, I.; Rozas, I.; Elguero, *J. Chem. Soc. Rev*., **1998**, 27, 163-170.

[42] McAfee, K. B.; Hughes, R. H.; Wilson Jr., E. B. *Rev. Sci. Instrum*. **1949**, 20, 821-826.

[43] Dyke, T.R.; Howard, B. J.; Klemperer, W. *J.Chem.Phys*. **1972**, 56, 2442.

[44] Balle, J.; Flygare, W. H. *Rev. Sci. Instrum*. **1981**, 52, 33 – 45.

[45]Brown, G. G.; Dian, B. C.; Douglass, K. O.; Geyer, S. M.; Pate, B. H. *J. Mol. Spectrosc*. **2006**, 238, 200-212.

[46] Park, S-W.; Kaimoyo, E.; Kumar, D.; Mosher, S.; Klessig, D.F. Science **2007**, 318, 113-116.

[47] Shulaev, V.; Silverman, P.; Raskin, I. *Nature* **1997,** 385, 718-721.

[48] Liyana-Arachi, T. P.; Hansel, A. K.; Stevens, C.; Ehrenhauser, F. S.; Valsaraj, K. T.; Hung, F. R. *J. Phys. Chem.* A **2013**, 117, 4436−4443.

[49] Richards-Henderson, N. K; Pham, A.T.; Kirk, B. B.; Anastasio, C. Environ. Sci. Technol. **2015**, 49, 268-276.

[50] Weller, A. *Z. Elektrochem.* **1956**, 60, 1144−1147.

[51] Klöpffer, W.; Kaufmann, G. J. Lumin. 1979, 20, 283−289.

[52] Lopez-Delgado, R.; Sylvain, L. *J. Phys. Chem.* **1981**, 85, 763−768.

[53] Helmbrook, L.; Kenny, J. E.; Kohler, B. E.; Scott, G. W. *J. Phys. Chem.* **1983**, 87, 280−289.

[54] Goodman, J.; Brus, L. E. *J. Am. Chem. Soc.* **1978**, 100, 7472−7474.

[55] Catalán, J.; Palomar, J.; dePaz, J. L. G. *J. Phys. Chem.* A **1997**, 101, 7914−7921.

[56] Zhou, P.; Hoffmann, M. R.; Han, K.; He, G. *J. Phys. Chem.* B, **2015**, 119, 2125–2131.

Chapter 2

Theoretical and Experimental Details

2.1 Theoretical Studies

2.1.1 ab initio Calculations

a) Background

In Chapter 1.1.3, the stepwise development of the various theoretical models to understand the nature of the H-bonding interaction was discussed. In particular, I pointed out that the application of high level ab initio quantum mechanical calculations can provide reliable structural and energetic descriptions of this interaction, which are in good agreement with experimentally derived results. In this section, a detailed analysis of the various levels of the ab initio calculation and the relevant basis sets are discussed.

In quantum chemistry, the energy of a molecule is obtained by solving the Schrödinger equation.

$$\hat{H} \quad = E \qquad 2.1$$

Here, $\hat{H}$ is the Hamilton operator and is the electronic wave function of the system. The operator $\hat{H}$ is the summation of kinetic energy (T) and potential energy (V) operators. In the Born-Oppenheimer approximation, the time independent Schrödinger equation for an n-particle system can be written as,

$$-\sum_{i=1}^{n} \frac{h^2}{8\pi^2 m_i} \nabla^2 \quad + V(x_i, y_i, z_i, \ldots\ldots\ldots, x_n, y_n, z_n) \quad = E \qquad 2.2$$

An analytical solution of the above equation is not possible, but approximate solutions can be obtained using numerical methods. In the Hartree Fock method, is the product of monoelectronic functions (spin orbitals), each describing the motion of an electron in a coulombian electric field produced by rest of the electrons and nuclei. The HF method is a variational method by which can be obtained after solving a number of integrals. A shortcoming of the Hatree Fock method is that it neglects electron correlation, resulting in large deviations from experimental results, in particular if *inter*molecular interactions are involved. To improve the HF method, several post HF methods such as MP2, MP4, coupled cluster etc. have been developed. All of these methods consider electron correlation, which was absent in the HF method.

(b) Level of Theory

Among the different post HF methods, the MP2 method is widely applied to H-bonded system because of its proven performance for such systems.[1,2] In the MP2 method, electron correlation is introduced by adding a perturbation to the Fock operator. Higher levels of theory, such as MP4, CCSD, or CCSD(T) are computationally more demanding. Alternatively, Density Functional Theory (DFT) is found to give very good results with more modest computational costs. The B3LYP functional performs well in terms of structures and relative energies of H-bonded conformers.[3]

In wavefunction-based ab initio calculations, molecular orbitals are constructed by linear combination of basis functions. A judicious selection of basis sets, sets of basis functions, is important to obtain reliable results. The basis sets used in this work include diffuse functions, i.e. functions, which decay slowly with distance. Diffuse functions are essential to properly describe hydrogen bonding, for example. The diffuse functions are indicated with '++' in the Pople type basis sets (e.g. 6-31G++(d,p), 6-311G++(2d,p)). In case of correlation-consistent basis sets (e.g. cc-pvDZ, cc-pVTZ) augmented versions are also used with added diffusion function (e.g. aug- cc-pvDZ, aug-cc-pVTZ). Ab initio *inter*molecular interaction energies are often calculated using the supermolecular approach, where the energies of the subunits are determined individually, and then subtracted from the energy of the entire complex. In this approach, the so-called basis set superposition error (BSSE) occurs, because the monomer units in the complex can make use of the basis sets of all other subunits, which results in a lowering of the energy. There are different methods to minimize this error; among them, the counterpoise correction scheme (CP) suggested by Boys and Bernardi[4] is the most used approach.

2.2. Experimental Details and analysis of Data

2.2.1 Introduction

Microwave spectroscopy coupled with a molecular jet expansion is one of the most powerful techniques which provides high resolution spectra of the molecular clusters. For my project I have used a narrowband cavity based molecular beam Fourier transform microwave (FTMW) spectrometer and broadband FTMW spectrometer. Both instruments use a pulsed nozzle to generate a supersonic beam expansion. Details about the supersonic beam expansion and about the spectrometers are discussed in this chapter. I used several rotational

spectroscopic programs for spectral assignments and analyses, which are also discussed in this chapter.

2.2.2 Supersonic beam expansion

At room temperature, many rotational energy levels are accessible in polyatomic molecules. As a result, the spectra can be so complex that it is very difficult, if not impossible, to achieve a spectroscopic assignment. The ideal solution would be to do spectroscopy of molecules at very low temperature. At low temperature, only few energy levels are populated. As a result, fewer transitions are detectable, thus greatly simplifying the spectra. However, under normal conditions cooling of gases leads to liquefaction and solidification. In the liquid and solid phases, transitions are generally unresolved as collisions lead to broadening of the energy levels. So, one should try to cool the gas to very low temperature in a collisionless environment. By using a supersonic beam expansion one can easily achieve these conditions.

In 1951 Kantrowitz and Gray[5] first proposed that the intensity of molecular beams can be increased in a supersonic beam expansion, which also leads to cooling. The components for the supersonic jet expansions are a gas reservoir, a valve, and an evacuated sample cell. In this case a gas at a temperature T_0 and pressure P_0 is expanded through a small hole or nozzle into a vacuum chamber. Before expansion, the velocity distribution of a gas can be described by the Maxwell Boltzmann distribution which depends on the initial temperature of the gas T_0. In the case of an effusive expansion, the diameter of the nozzle is smaller than the mean free path of the gas. As a result, the molecule can go through the nozzle hole without any collision, which means that the velocity distribution before and after the expansion is the same. In case of effusive expansion there will be no cooling of the sample gas.

An interesting effect occurs if the nozzle diameter is much larger than the mean free path of the gas. In that case there will be many collisions between the molecules in the nozzle orifice. As a result, only those molecules which have a large velocity component in the direction to the vacuum will escape. Due to the collisions the velocity distribution of the gas will narrow down and also most of the molecules will travel at the same velocity in the same direction after the expansion. In case of a monoatomic gas, as there are no vibrational and rotational degrees of freedom, the supersonic expansion leads to translational cooling of the molecules. If a small amount of any other molecule is added with the noble gas or carrier gas, there will be collisions between the noble gas atoms and the molecules, resulting in the velocity

distribution of the molecules also to narrow down. Before the expansion, all the degrees of freedom of the molecule are in equilibrium and, as a result, the vibrational temperature, measured from the populations of different vibrational states (using the Boltzmann distribution) will be same as the rotational and translational temperatures. This equilibrium will be lost after the expansion. During the collision, vibrational and rotational energy of the molecule will be transferred to the translational energy of the carrier gas. Rotational levels will be depopulated much more efficiently than vibrational energy levels because smaller quanta of energy are easier to remove. After the expansion, the molecules and carrier gas travel at the same velocity, such that there will be essentially no collisions. In the collisionless region, the equilibrium between the degrees of freedom is lost and, as a result, there will be different translational, rotational, and vibrational temperatures of the molecules. During expansion the molecules mainly collide with noble gas atoms and after expansion, in the collision free region, liquefaction or solidification does not occur and the molecule persists at very low temperature for a long time. Generally, the amount of cooling depends on different parameters such as initial pressure, the nozzle diameter, identity of the carrier gas, and final pressure.

So, in a supersonic jet expansion only few energy levels are accessible due to cooling, and the molecular spectra are simplified and easier to sort out.

2.3 Microwave Spectroscopy

In pure rotational spectroscopy, microwave radiation ($0.01 cm^{-1}$ – $100\ cm^{-1}$ or 0.3 - 3000 GHz) is used to measure the energies of rotational transitions of molecules. Depending on the shape and moments of inertia about the rotational axes, molecules can be divided into five categories. Details about the different types of molecules, theory of rotational spectroscopy, and different spectrometers are discussed in this section.

2.3.1 Theory of Rotational Spectroscopy

When a molecule is irradiated with microwave radiation, it can absorb a photon through the interaction of its electric dipole moment and the photon's electric field. If the photon energy is similar to energy gap between two rotational energy levels there may be a rotational transition. The interaction between a molecule and radiation depends on the transition dipole moment as follows,

Transition dipole moment or probability of transition = $\int \Psi_f^* \hat{\mu}_g \Psi_i \, d\tau$

Here, Ψ_f^* is the complex conjugate of the final excited state rotational wave function, Ψ_i is the rotational wave function of the initial state and $\hat{\mu}_g$ is the dipole moment operator in the cartesian coordinate g (g can be x, y or z) axis. The intensity of a transition depends on transition dipole moment. The projection of the dipole moment along the axis of the electric field has to be non-zero in order for the transition to occur. Another important criterion in rotation spectroscopy concerns the orthogonality of the initial and final wave function Ψ_i and Ψ_f. As the photon contains one unit of angular momentum, it can provide only one unit of angular momentum to the molecule during interaction. This restricts the rotational transition to happen between the rotational levels that differ by only one unit in the rotational quantum number J, i.e.

$$\Delta J = \pm 1 \qquad 2.3$$

Selection rules and transition moment integrals decide whether the transition is allowed or not but this does not take into account the population of the rotational states which also determines the intensity of the rotational transition. In this aspect, the Boltzmann distribution can be used to determine the population of molecules in different states for a particular temperature. This can be written as,

$$\frac{n_j}{n_0} = \frac{e^{(-E_{rot}(J)/RT)}}{\sum_{J=1}^{J=n} e^{(-E_{rot}(J)/RT)}} \qquad 2.4$$

Here, $E_{rot(J)}$ is the rotational energy of the state with rotational quantum number J of the molecule. n_j is the number of molecules in the j^{th} energy state, n_0 is the total number of molecules. T is the rotational temperature of the sample. According to this distribution, the peak corresponding to the transition from the energy state with the largest population will be the largest.

2.3.2. Rigid Rotor

In most cases rotational spectra of molecules can be described using a rigid rotor model, according to which, for example, a diatomic molecule rotates about its center of mass (c.o.m.) and the distance between the atoms does not change during rotation. Energy levels of the rigid rotor can be obtained as eigenvalues by solving the Schrödinger equation with a

properly formulated energy operator. The time independent Schrödinger equation can be written as,

$$\hat{H}_0\psi = \mathrm{E}\psi(\mathrm{q}) \qquad 2.5$$

And in spherical coordinates,

$$-\frac{\hbar^2}{2\hat{I}}\left[\frac{1}{sin\theta}\frac{\partial}{\partial\theta}\left(sin\theta\,\frac{\partial}{\partial\theta}\right)+\frac{1}{sin^2\theta}\left(\frac{\partial^2}{\partial\phi^2}\right)\right]\quad(\theta)\quad(\phi)=\mathrm{E}\quad(\theta)\quad(\phi) \qquad 2.6$$

Here $\hat{I}$ is the moment of inertia, solutions to θ and ϕ equations give (θ) and (ϕ) respectively, where $\theta$and ϕ are angular coordinates. The product (θ) (ϕ) are the spherical harmonics, which are often denoted as Y. The above equation is solved after separation of variables, which gives the eigenfunction Y as,

$$\mathrm{Y_J^M}(\theta,\phi) = N_{JM}\,P_J^{|M|}(\cos\theta)\,e^{iM\phi} \qquad 2.7$$

$P_J^{|M|}$is the associated Legendre polynomial and N_{JM} is a normalization constant.

$$N_{JM} = \left(\frac{(2J+1)(J-|M|)!}{4\pi(J+|M|)!}\right)^{1/2} \qquad 2.8$$

The energy values for the rigid rotor are given by

$$E_J = \frac{\hbar^2}{2\hat{I}}\,\mathrm{J(J+1)} = \mathrm{BJ(J+1)} \qquad 2.9$$

E_J is the energy value for the rotational level with quantum number J. It is to be noted that the quantum number M does not affect the energy values and that each rotational state is (2J+1) fold degenerate. In presence of an external magnetic or electric field this degeneracy is lost, which is termed as Zeeman (magnetic) or Stark (electric) effect.

2.3.4 Rotational Symmetry

In rotational spectroscopy molecules can be divided into 5 different categories, depending upon their moments of inertia about the three rotational axes: linear molecules e.g. HCN (I_B=I_C, I_A=0), spherical tops e.g. SF_6 (I_A=I_B=I_C), prolate symmetric tops e.g. CH_3Cl (I_A<I_B=I_C), oblate symmetric tops e.g. BF_3 (I_A=I_B<I_C), asymmetric tops e.g. H_2O (I_A<I_B<I_C). Details about the different types of molecules, their Hamiltonian and solutions are given in

Ref [6] and Ref [7]. Here I have just concentrated on the energy values of different type of molecules.

The energy values of the linear and diatomic molecules were already discussed in the previous section. The energy values of the symmetric tops are given by

$$E_{JK}= BJ(J+1)+ (A-B)K^2 \quad \text{(Prolate top)} \qquad 2.10$$

$$E_{JK}= BJ(J+1)+ (C-B)K^2 \quad \text{(Oblate top)} \qquad 2.11$$

The quantum number K is associated with the rotation about the principal rotational axis and the values of A, B, C are given below,

$$A= \frac{h^2}{8\pi^2 I_A} \qquad 2.12$$

$$B= \frac{h^2}{8\pi^2 I_B} \qquad 2.13$$

$$C= \frac{h^2}{8\pi^2 I_C} \qquad 2.14$$

The energy levels for the symmetric top also do not depend on the quantum number M. The selection rules for symmetric tops are, $\Delta J=\pm 1$, $\Delta M= 0, \pm 1$ and $\Delta K= 0$.

The asymmetric top Hamiltonian is solved by using a symmetric top basis set. The energy levels of the rotational levels are denoted as $J_{K_a K_C}$, where J is a good quantum number but K_a and K_C are just labels and they become good quantum number in the prolate and oblate symmetric top limits, respectively. The selection rules for an asymmetric top molecule are given as follows. For all types of asymmetric top molecules, the selection rules in J and M are $\Delta J= 0,\pm 1$ and $\Delta M= 0, \pm 1$. However, the selection rules in K_a and K_c depend on the dipole moment components (μ_a, μ_b and μ_c) along the principal inertial axes of the molecule. Depending on the values of these components, transitions are classified into three groups, i.e. a-type, b-type and c-type transitions.

For a-type transitions with $\mu_a \neq 0$:

$$\Delta K_a= 0 (\pm 2, \pm 4..) \text{ and } \Delta K_c = 1 (\pm 1, \pm 3 ...) \qquad 2.15$$

For b-type transitions with $\mu_b \neq 0$:

$$\Delta K_a= \pm 1 (\pm 3, ...) \text{ and } \Delta K_c = \pm 1 (\pm 3, ...) \qquad 2.16$$

For c-type transitions with $\mu_c \neq 0$:

$$\Delta K_a = \pm 1\ (\pm 3, ...) \text{ and } \Delta K_c = 0\ (\pm 2, ...) \qquad 2.17$$

2.4 Spectrometers

For the experimental studies, I have used two types of microwave spectrometers. One is a cavity based Fourier transform microwave spectrometer, which is capable of measuring a narrow frequency bandwidth with high resolution and the other one is chirped pulse Fourier transform microwave spectrometer, which is capable of measuring a broad frequency bandwidth spectrum. Details about the spectrometers are discussed below.

2.4.1 Cavity-Based Fourier Transform Microwave Spectrometer

Several kinds of microwave spectrometers, such as a Stark modulation instrument with wave guide sample cell, have been used to study molecular structure.[8, 9] FTMW spectroscopy was first established by Flygare and McGurk[10] in the 1970s and early 80s. Later, Flygare[11] has modified the instrument by incorporating a Fabry-Perot cavity and a pulsed supersonic expansion. The Fabry-Perot cavity consists of a pair of spherical mirrors, situated inside a vacuum chamber, which acts as a sample cell. The sample was introduced as a supersonic beam expansion by a pulsed nozzle. This new spectrometer, referred to as a Balle-Flygare spectrometer, provides a much higher resolution and also allows the generation of clusters of various sizes with low vibrational and rotational temperature. Below a brief description of the Balle-Flygare spectrometer which is used in the Jäger lab, is described. More detailed descriptions of the spectrometer are given in Ref [12] and Ref [13].

(a) Theoretical Description

The experimental technique of FTMW spectroscopy is based on the pulsed microwave excitation of an ensemble of molecules and subsequent detection of the coherent spontaneous molecular emission signal. The instrument relies on an intense coherent microwave pulse, which aligns the initially randomly oriented electric dipoles to rotate in phase with each other and generate a macroscopic polarization of the gas sample (Fig 2.1). If the initial microwave pulse has a frequency resonant with a molecular transition, and the pulse width is shorter than any relaxation processes, then, once the incident pulse has dissipated, the macroscopic polarization decays at a rate T_2 and emits coherent radiation at the transition frequency. The

emitted signals are collected as free induction decay and then averaged with subsequent emission signals and finally Fourier transformed to obtain the frequency domain signal.

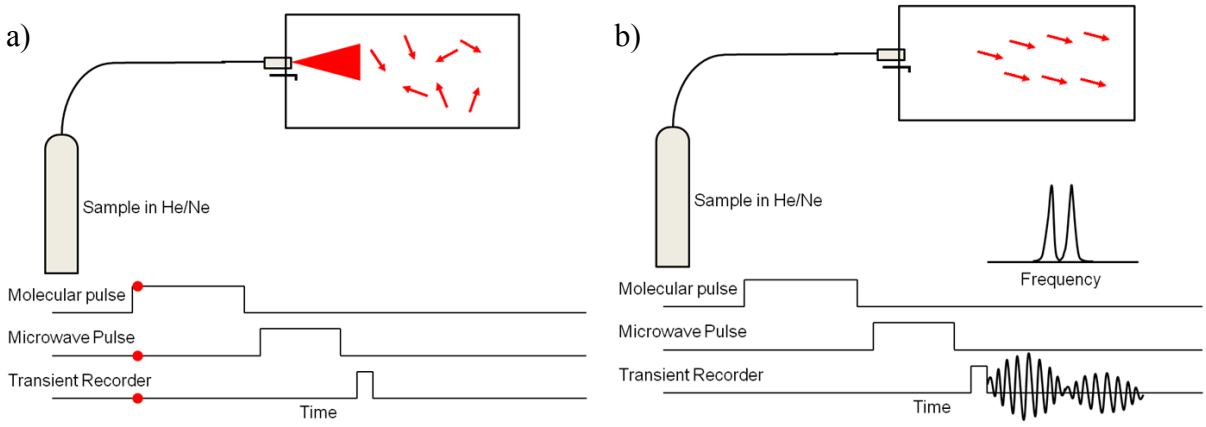

Fig 2.1 Theoretical background of the FTMW spectroscopic technique. a) before and b) after the microwave excitation pulse.

The theoretical treatment of FTMW spectroscopy is concerned with the responses of a two-level quantum particle with the electromagnetic field, similar as in the case of Fourier-transform NMR spectroscopy. The short lived responses of the system are termed *transient phenomena* and can be described by the optical Bloch equations.[14] The application of the microwave pulse causes the mixing of the wavefunctions of two rotational states of the molecule and generates a superposition state. If one applies a $\pi/2$ microwave excitation pulse, it reduces the initial population difference between two levels so that both the levels are equally populated. As a result of the $\pi/2$ pulse ($\omega_R t = \pi/2$, where ω_R is Rabi frequency and t is time), the initial population difference converts into a macroscopic polarization. The macroscopic polarization of the molecular ensemble depends on the Rabi frequency, which is the product of the strength of the electric field of the microwave radiation and the electric dipole moment for a given transition. For a transition $i \rightarrow f$, the Rabi frequency is given by

$$\omega_R = \mu_{f \leftarrow i} \varepsilon / \hbar \qquad 2.18$$

Here, ω_R is the Rabi frequency and $\mu_{f \leftarrow i}$ is the electric dipole moment of the transition between levels i and f, and ε is the electric field amplitude of the MW radiation. For a molecule with a small dipole moment, a microwave power amplifier is often used to boost the excitation pulse power.

(b) Instrument design

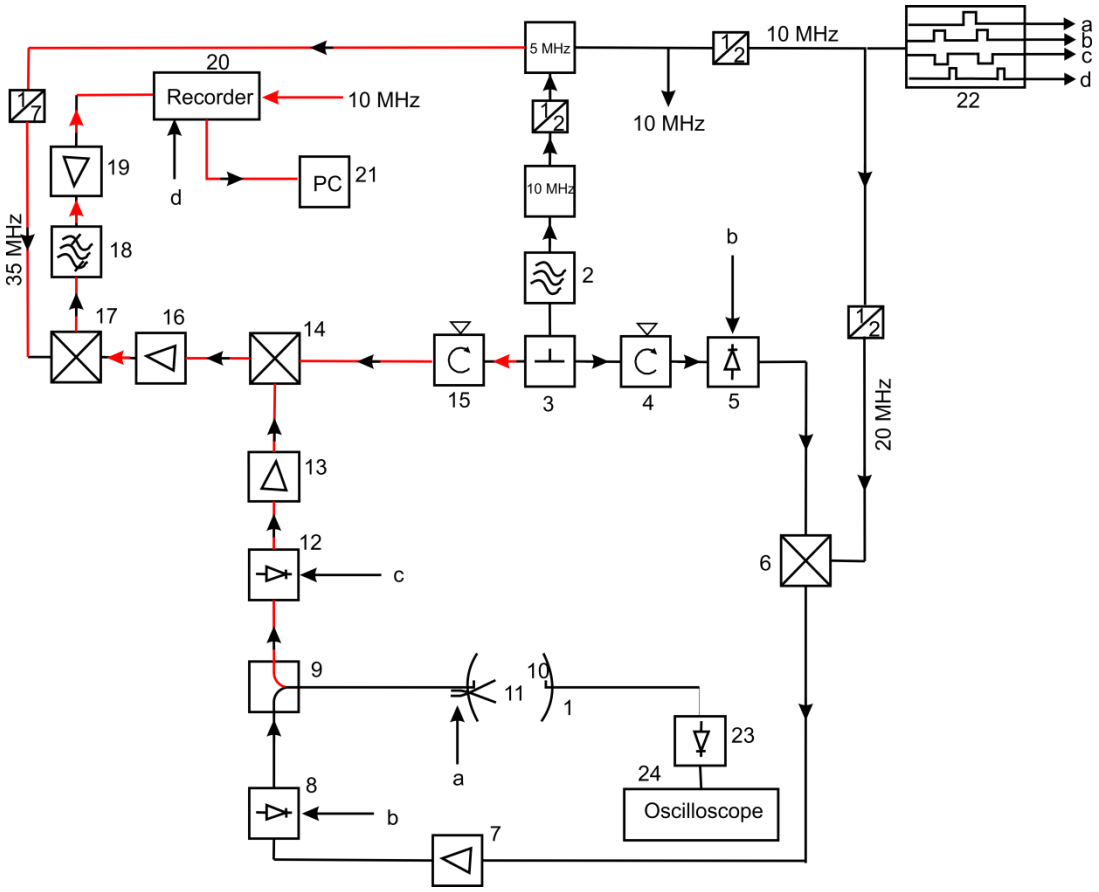

Figure 2.2 A schematic diagram of the Balle-Flygare Fourier Transform Spectrometer (derived from Ref [15]).

The components of the Spectrometer are (1) nozzle, (2) Hewlett Packard MW synthesizer, (3) power divider, (4) isolator, (5) MW PIN switch, (6) 20 MHz double balanced mixer, (7) MW power amplifier, (8) MW PIN switch, (9) circulator, (10) antenna, (11) MW cavity, (12) MW PIN switch, (13) MW power amplifier, (14) image rejection mixer, (15) isolator, (16) radio frequency (RF) amplifier, (17) RF mixer, (18) 15 MHz band pass filter, (19) RF amplifier, (20) transient recorder, (21) personal computer, (22) pulse generator, and (23) detector.

In the above diagram black arrows show the excitation part and the red arrows denote the detection part of the system. Depending on the function, the whole set up can be divided into three major parts: (I) excitation arm, (II) sample cell or cavity, (III) detection system.

(I) Excitation arm

Like other spectrometers, this spectrometer needs excitation radiation to excite the molecules. The coherent microwave excitation radiation is produced by a MW synthesizer

(2). The microwave radiation is divided into two arms using a power divider (3). One arm is used to generate the excitation pulse. A MW pin switch (5) is used to produce the MW excitation pulse. Afterwards, it is mixed with a 20 MHz signal using a double balanced mixer (6) which produces two sidebands, offset by 20 MHz from the original MW frequency. This offset is used in the heterodyne detection process to produce signals around 20 MHz. The excitation pulse is then passed through another MW pin switch (8) before the MW pulse is introduced into the cavity through an L shaped antenna.

(II) Sample cell or microwave cavity

In this spectrometer, two spherical aluminium mirrors form a microwave cavity; it also serves as the sample cell. The diameter of the mirror is 26 cm and radius of curvature is 38 cm. The distance between the mirrors is between 20 and 40 cm. The position of one of the mirrors is fixed and the other mirror is adjusted using a computer controlled motor, in order to tune the cavity into resonance with the external microwave radiation. The corresponding standing wave of the incident microwave radiation is collected by another L shaped antenna situated at the middle of the movable mirror and the microwave power fed through the cavity is monitored by a microwave detector and an oscilloscope (24).

There are some great advantages of the Fabry-Perot cavity. The MW cavity accepts only certain frequencies, which depend on the specific mirror separation. All other frequencies interfere destructively and are reflected. The cavity acts thus as a filter. Another important advantage of the cavity is that the quality factor (Q), defined as the ratio of the energy stored in the resonator to the power dissipation, is very high. For a frequency of 10 GHz, the typical bandwidth of the cavity is about 1 MHz and a typical value of the quality factor is about 10^4.

The sample is introduced as a supersonic beam expansion through a nozzle (1) situated at the center of the stationary mirror. In our spectrometer the path of the molecular beam is parallel to the microwave propagation direction, i.e. parallel to the cavity axis. As a result of this, all the rotational lines split into two Doppler components. The coaxial arrangement allows the molecules to interact with the microwave radiation for a longer time, which reduces the spectral line width to a few KHz. The low pressure of the chamber is maintained by using a 12-inch diffusion pump connected to the microwave cavity. A backing pump is used as a fore pump.

(III) Detection system

After the excitation of the molecular ensemble, it emits the radiation which can be represented as ν-20MHz+$\Delta\nu_m$, where $\Delta\nu_m$ is the offset from the excitation frequency. The emission signal is collected by the same L shaped antenna connected to the fixed mirror. The emission signal is then sent to the detection arm through a circulator (9). After that, the signal goes through a MW PIN diode switch (12) which protects the electronic components from the high power microwave excitation pulse. The signal is then amplified by using a low-noise MW amplifier (13). The amplified signal is then mixed with the original microwave frequency (ν) by using an image rejection mixer (14) to give an intermediate frequency of 20 MHz + $\Delta\nu_m$, which is then mixed with 35 MHz to a 15 MHz + $\Delta\nu_m$ intermediate frequency by using a RF frequency mixer. The final frequency is then passed through a 15 MHz band pass filter before the time domain signal is digitized with a transient A/D recorder and Fourier transformed to get the frequency power spectrum.

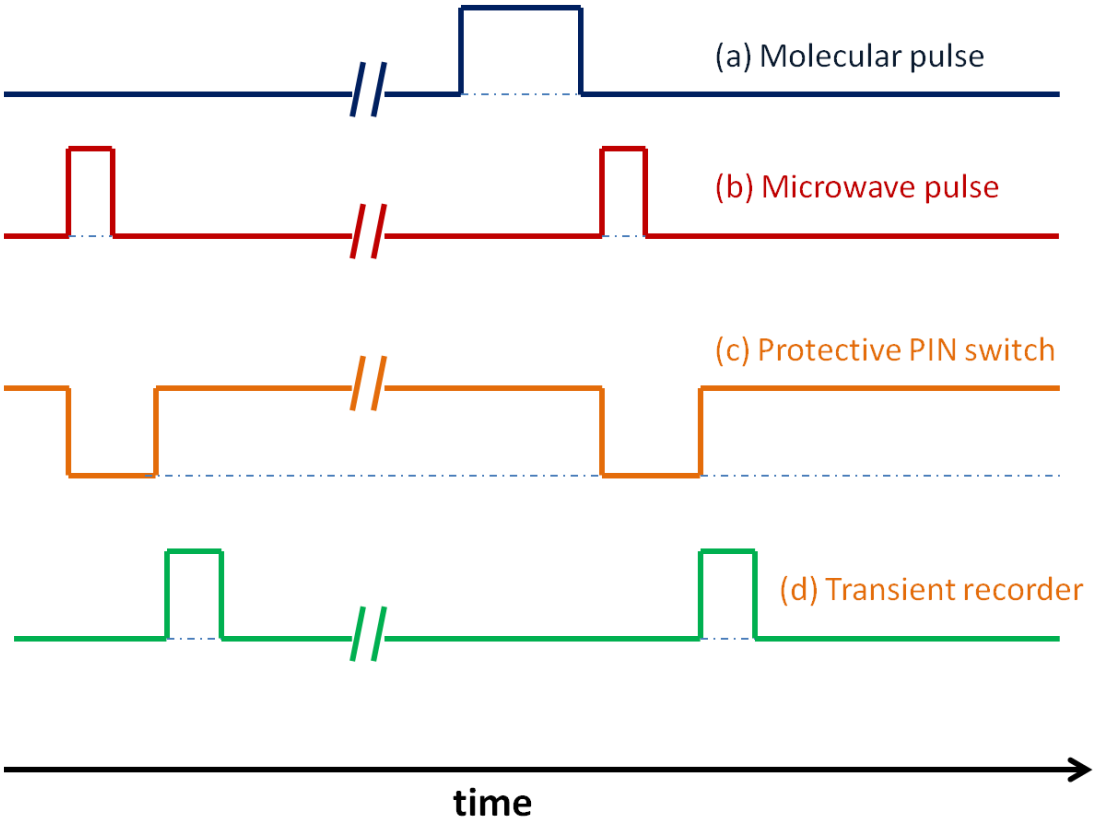

Figure 2.3 A typical pulse sequence used in the cavity based FTMW spectrometer.

The performance of the spectrometer depends on the proper timings of several events that occur during each averaging cycle. The timing of the events is controlled by transistor-

transistor-logic or TTL pulses as shown in figure 2.3. In the diagram, line (a) represents the "molecular pulse" which indicates opening of the nozzle, generally for 400-900 μs. Line (b) denotes the "microwave pulse" which is generated after 10 μ delay of the molecular pulse. Simultaneously the protective switch switches into the high loss state (as shown by line (c)) to protect the detection system from the high excitation microwave power. The protected switch is then set to a low loss state after the power inside the microwave resonator has decreased sufficiently and data acquisition begins at this point.

2.4.2 Chirped Pulse Fourier Transform Microwave Spectrometer

A cavity based FTMW spectrometer has many great advantages, such as high resolution and high sensitivity due to the use of the resonator, which reduces the power requirement of the excitation pulse. Unfortunately, however, use of the resonator limits the bandwidth of the spectrometer to about 1 MHz. Generally, measuring a spectrum using a cavity based FTMW spectrometer always requires tuning of the cavity mirrors into resonance with the excitation frequency and unfortunately this takes most of the experiment time. In fact the bandwidth of this type of spectrometer is about 1 MHz and it takes more than 12 hours to measure a region of about 100 MHz.

In 2006, the Pate group[16] at the University of Virginia developed a FTMW spectrometer that is capable of measuring 11 GHz of bandwidth in less than 10 μs, for a single averaging cycle. This instrument is called a chirped-pulse Fourier transform microwave spectrometer (CP-FTMW). The main advantages of this spectrometer, such as the bandwidth and acquisition speed make this spectrometer very useful for the molecular spectroscopy community.

There are three major components of the chirped pulse FTMW spectrometer which make the spectrometer so special. Those are a high speed digitizer (40 Gsamples/sec) for acquisition of the microwave emission, a broadband high power amplifier to provide the required amount of power to polarize the molecules, and an arbitrary waveform generator (AWGs) to produce a chirped microwave excitation pulse of few GHz bandwidth of short duration (several μs). Recently, the Jäger[17] group has developed a CP-FTMW spectrometer based on the previously reported design, which I have used for my research studies. A schematic diagram of the spectrometer is given in Figure 2.3.

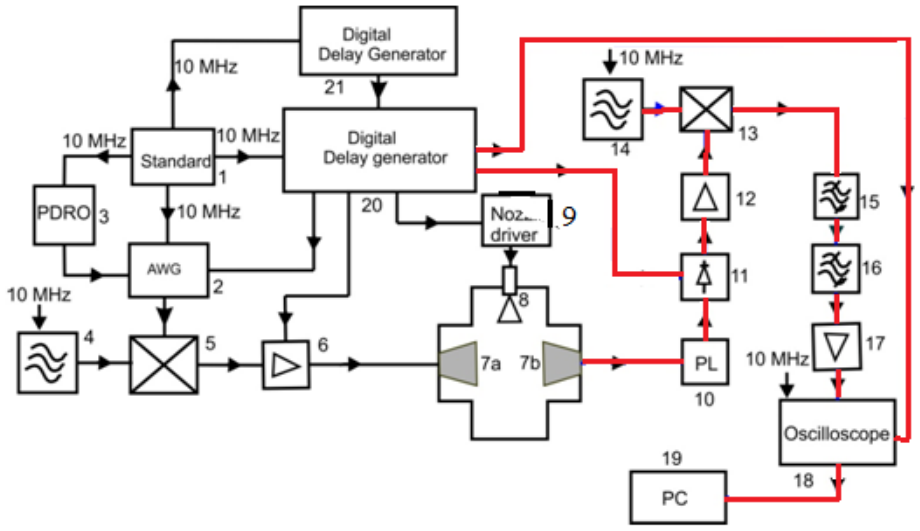

Figure 2.4 A schematic diagram of the Chirped Pulse Fourier Transform Spectrometer (derived from Ref 12).

All the components of the spectrometer are given below.

(1) Rb frequency standard, (2) arbitrary waveform generator, (3) 3.96 GHz phase-locked dielectric resonator oscillator (PDRO), (4) synthesizer 1, (5) double balanced mixer, (6) 20 W solid state amplifier, (7) high gain horn antennas, (8) nozzle, (9) nozzle driver, (10) power limiter, (11) PIN diode switch, (12) low noise amplifier, (13) double balanced mixer, (14) synthesizer 2, (15) low pass filter, (16) low pass filter (17) low noise amplifier, (18) oscilloscope, (19) personal computer, (20) digital delay generator, and another (21) digital delay generator.

In the above diagram black arrows show the excitation part and the red arrows denote the detection part of the system. Depending on the functions, the whole set up can be divided into three major parts: (I) chirp excitation pulse generation, (II) sample cell, (III) detection system.

(I) Chirped Pulse Generation

One of the essential parts of the CP-FTMW spectrometer is generation of a broadband chirped pulse of short duration, typically several μs. In a chirped pulse, the frequency changes during the pulse in a pre-determined fashion. It is generated by a 4.2 Giga samples/s arbitrary wave form generator (AWG) (2), which is referenced to an external phase locked dielectric resonator oscillator (PDRO) (4) that operate at 3.96 GHz. The AWG produces a 4 μs chirped pulse with a bandwidth from 0.2 GHz to 1 GHz ($\Delta\nu$). The resultant chirped pulse ($\Delta\nu$) is then mixed with a fixed MW frequency (ν_{MW}), generated by microwave synthesizer (4) by using a

double balanced mixer (5). The mixing process gives a chirped pulse of $\nu_{MW} \pm \Delta\nu$, with a frequency width of 2 GHz centered at ν_{MW}. Depending on the ν_{MW} one can set the frequency value to the desired frequency range. Unlike the cavity based FTMW spectrometer, the CP-FTMW spectrometer has no resonator to store enough power, which is necessary to excite the molecules in a large frequency range. Instead, the chirped microwave pulse is amplified by using a 20 W high-power solid state amplifier (6). The amplified pulse is then broadcast into an evacuated chamber through a horn antenna (7).

(II) Sample Chamber

The sample cell of CP-FTMW spectrometer in our lab consists of a six-way cross aluminium chamber. The sample is introduced as a supersonic beam expansion through a pulsed nozzle. Unlike in the cavity based FTMW spectrometer the molecular jet expansion occurs perpendicular to the propagation direction of the microwave radiation. Two identical microwave horn antennas (7) separated by 30 cm are used to broadcast the high power amplified chirped pulse and to collect the emission signal, respectively. One of the significant differences between the cavity based FTMW and CP-FTMW spectrometer is that the interaction time between the molecular ensemble and excitation pulse as well as the time to detect the molecular emission is less in case of CP-FTMW due to the perpendicular orientation of chirped pulse and molecular beam, though the Doppler splitting is reduced due to this type of orientation. The sample chamber is connected to a 1300 L/s diffusion pump to maintain a low pressure of about 1 mTorr in the chamber. A backing pump is used to support the diffusion pump.

(III) Detection System

After it is collected by the high gain horn antenna, the emission signal is fed through a power limiter (10), an SPST PIN diode switch (11), and a low noise microwave amplifier (12). The task of the power limiter and the SPST PIN diode switch is to protect the low noise amplifier from the high power chirped excitation pulse. After the low noise amplifier, the signal at frequencies $\nu_{MW} \pm \Delta\nu$ is mixed with a microwave frequency that is 1.5 GHz higher than the center frequency ν_{MW} to prevent folding of the rotational spectrum. The resultant signal is then filtered with a 4.4 GHz low pass filter (15) to remove any high frequency artifacts present in the signal. The final signal is then digitized by a fast digital storage oscilloscope (18) after passing through another low noise amplifier (17). The oscilloscope can digitize the

time domain signal at a rate of 40 Gsamples/sec and a vertical resolution of 8 bit. The data set is transferred to a computer and averaged there for signal improvement. The averaged time domain signal is then Fourier transformed to obtain a frequency domain signal. An example of a broadband spectrum of a sample mixture of methyl Salicylate and water is shown is figure 2.5.

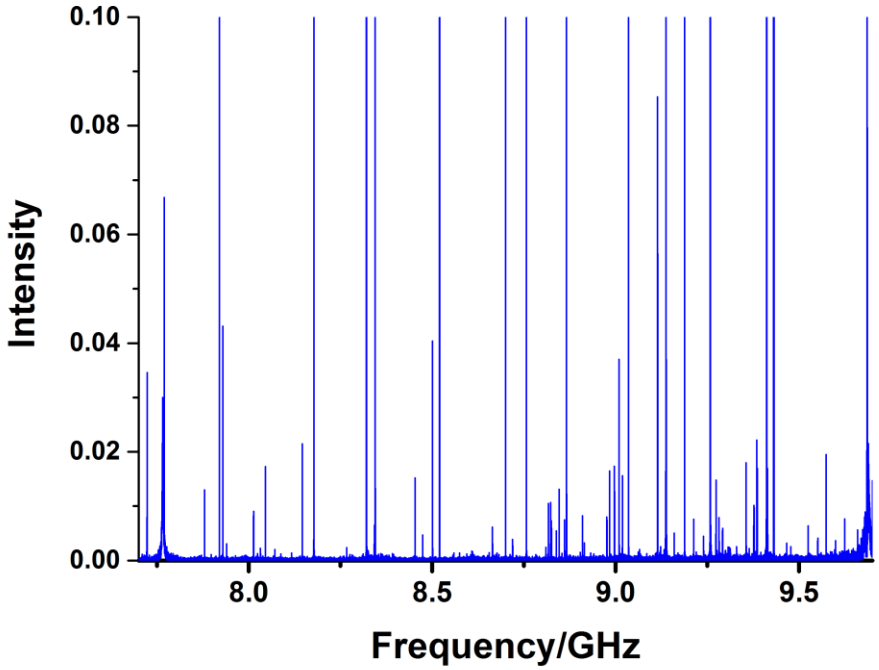

Figure 2.5 A broadband spectrum of methyl salicylate and water using our chirped pulse FTMW spectrometer at a center frequency of 8.7 GHz. Details about the experimental conditions are discussed in Chapter 3.

Like the cavity instrument, the chirped FTMW spectrometer also requires a proper timing sequence to achieve the phase stability of the time domain signal for averaging. The operation of the different components of the spectrometer such as pulsed nozzle, AWG, high power amplifier, protective switches and digital oscilloscope are controlled by TTL signals generated by a pulse generator. The pulse sequence used in our CP-FTMW spectrometer is shown in Figure 2.5. One experimental cycle is consisted of one such pulse sequence.

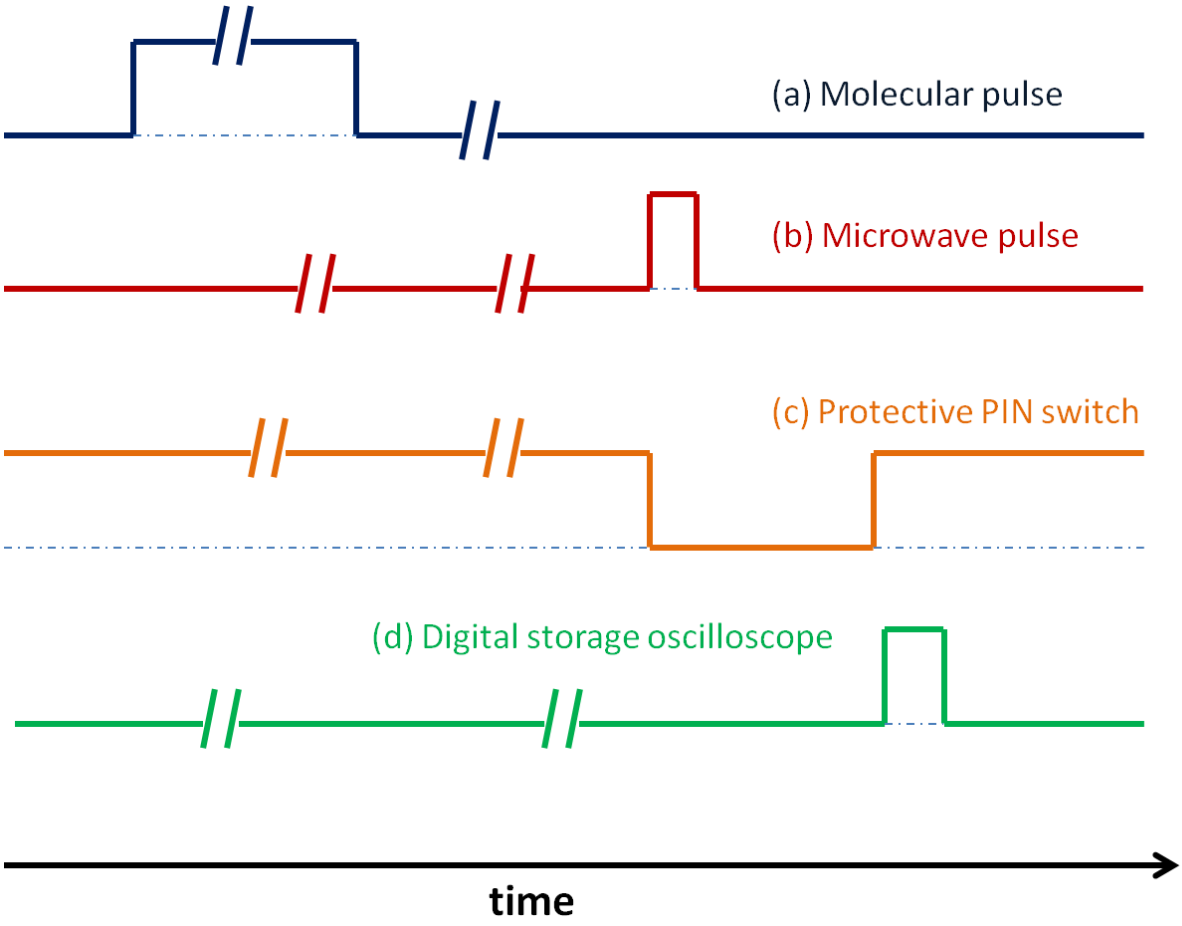

Figure 2.6 A typical pulse sequence used in the chirped pulse FTMW spectrometer. (a) Molecular Pulse (500-900 μs), (b) Microwave pulse (0.5-3.5 μs), Protective PIN diode switch (6-12 μs), (d) Trigger for digital storage oscilloscope.

2.5 Analysis of the Spectra

In rotational spectroscopy, for assigning the spectrum of a molecule or a cluster of interest, a general strategy is often applied. Initially, an *ab initio* calculation is performed to determine a structure and thus rotational constants for the molecules or the cluster. My calculations were carried out using the Gaussian 09 suite of programs.[18] Details about the *ab initio* calculations of methyl salicylate and its water clusters are discussed in Chapter 3. The calculations gave rotational constants and dipole moment components of the optimized structure. Theoretical simulated spectra were obtained by using the constants for all the possible lower energy conformers in a spectral prediction program (Pgopher[19]).

Broadband scans were carried out for the methyl salicylate monomer and for methyl salicylate with water in our chirped pulse instrument. The theoretical spectra were then

compared with the experimental spectra. Once the spectral patterns were identified and rotational transitions assigned, individual peaks were measured using the cavity instrument.

A number of programs were used to simulate and fit the lines in the rotational spectra. For this study I have used Pgopher[19] and XIAM.[20] Pgopher is useful for analyses of hyperfine splitting due to nuclear quadrupole hyperfine structures, and XIAM is useful to fit hyperfine splitting for a molecular system with high internal rotor barrier. The results of the current study are discussed in chapter 3.

[1] Feng, G.; Gou, Q.; Evangelisti, L.; Xia, Z.; Caminati,W. *Phys. Chem. Chem. Phys.,* **2013,** 15, 2917.

[2] Tanjaroon, C,; Jäger, W. *J. Chem. Phys,* **2007**, 127, 34302.

[3] Evangelisti, L.; Ecija, Cocinero, J.; Castano, F.; Lesarri, A.; Caminati, W.; Meyer, R. J. *Phys. Chem. Lett*. **2012**, 3, 3770.

[4] Boys, S. F.; Bernardi, F. *Mol. Phys*. **1970**, 19, 553−566.

[5] Kantrowitz, A.; Grey, *J. Rev*. *Sci*. *Instrum.* **1951**, 22*,* 328-332.

[6] Townes, C.H.; Schawlow, A.L. Microwave Spectroscopy, Dover Publications, 1955.

[7] Bernath, P.F. Spectra of Atoms and Molecules, Oxford University Press, 1995.

[8] McAfee, K. B.; Hughes, R. H.; Wilson, E. B. *Rev. Sci. Instrum*. **1949**, 20, 821-826.

[9] Hughes, R. H.; Wilson, E. B. *Phys. Rev*. **1947**, 71, 562-563.

[10] McGurk, J. C.; Schmalz, T. G.; Flygare, W.H. *Density Matrix, Bloch Equation Description of Infrared and Microwave Transient Phenomena*; (eds.; In Prigogine, I.; Rice, S.A.), 1974.

[11] Balle, T. J.; Flygare, W. H. *Rev. Sci. Instrum*. **1981**, 52, 33 – 45.

[12] Xu, Y.; Jäger, W. *J. Chem. Phys*. **1997**, 106, 7968-7980.

[13] Xu, Y.; Wijngaarden, J. van.; Jäger, W. *Int. Rev. Phys. Chem*. **2005**, 24, 301- 338.

[14] Schmalz, T. G.; Flygare, W.H. Laser and Coherence Spectroscopy, (ed.; Steinfeld, J. I.) Plenum, New York, 1978, pp. 125–196.

[15] Thomas, J. Ph.D. Thesis, University of Alberta, 2014.

[16] Brown, G. G.; Dian, B. C.; Douglass, K. O.; Geyer, S. M.; Pate, B. H. *J. Mol. Spectrosc*. **2006**, 238, 200-212.

[17] Dempster, S.; Sukhorukov, O.; Lei, Q.-Y.; Jäger, W. *J. Chem. Phys*. **2012**, 137, 174303/1-8.

[18] Gaussian 09, Rev. C.01, M. J. Frisch, G. W. Trucks, H. B. Schlegel, G. E. Scuseria, M. A. Robb, J. R. Cheeseman, G. Scalmani, V. Barone, B. Mennucci, G. A. Petersson, H. Nakatsuji, M. Caricato, X. Li, H. P. Hratchian, A. F. Izmaylov, J. Bloino, G. Zheng, J. L. Sonnenberg, M. Hada, M.Ehara, K. Toyota, R. Fukuda, J. Hasegawa, M. Ishida, T. Nakajima, Y. Honda, O. Kitao, H. Nakai, T. Vreven, J. J. A. Montgomery, J. E. Peralta, F. Ogliaro, M. Bearpark, J. J. Heyd, E. Brothers, K. N. Kudin, V. N. Staroverov, T. Keith, R. Kobayashi, J. Normand, K. Raghavachari, A. Rendell, J.C. Burant, S. S. Iyengar, J. Tomasi, M. Cossi, N. Rega, J. M. Millam, M. Klene, J. E. Knox, J. B. Cross, V. Bakken, C. Adamo, J. Jaramillo, R. Gomperts, R. E. Stratmann, O. Yazyev, A. J. Austin, R. Cammi, C. Pomelli, J. W. Ochterski, R. L. Martin, K. Morokuma, V. G. Zakrzewski, G. A.Voth, P. Salvador, J. J. Dannenberg, S. Dapprich, A. D. Daniels, O. Farkas, J. B. Foresman, J. V. Ortiz, J. Cioslowski, D. J. Fox, Gaussian, Inc.,Wallingford CT, **2010.**

[19] Pgopher, a Program for Simulating Rotational Structure, C. M. Western, University of Bristol, http://Pgopher.chm.bris.ac.uk.

[20] Hartwig, H. Dreizler, *Z. Naturforsch*. **1996**, 51a, 923–932.

Chapter 3

Study of the Methyl Salicylate-Water Complex

*The work presented here has been reproduced in part from the following publication: Ghosh, S.; Thomas, J.; Huang, Wenyuan,; Xu, Yunjie,; Jäger, W. "Rotational Spectra of Two Hydrogen-Bonded Methyl Salicylate Monohydrates: Relative Stability and Tunneling Motions", *J. Phys. Chem. Lett.* **6**, 3126, 2015.

3.1 Introduction

The importance of methyl salicylate has already been discussed in Chapter 1. It was shown that methyl salicylate is an important molecule for medicine, biology, spectroscopy and even for the environment. The study of the interactions of methyl salicylate with water is of particular interest, as biological systems are typically aqueousIn its ground state methyl salicylate is a weak acid (pka=10.2), so in aqueous solution it can be expected that the *intra*molecular hydrogen bond that is present in the MS monomer is broken to form an *inter*molecular hydrogen bond with water molecules.

Another reason why studying MS water clusters is important is because of its effect on the environment.[1] While SOA formation is traditionally viewed as a gas-phase process, researchers have increasingly recognized the importance of SOA formation in atmospheric aqueous phases such as fog and cloud droplets and the resulting impact on air quality and fate of pollutants.[2,3] As discussed, MS being a VOC can be a precursor for SOA. Since the kinetics of SOA formation depends on the environment in which MS and oxidants react, it is important to know how MS interacts with water. Another significant property of volatile organic compounds is that they may act as surfactants, reducing the surface tension of cloud condensation nuclei (CCN), on which water condenses to form clouds. CCN can be different aerosol particles (such as black carbon from chimney or forest fire, sulfate, SOA etc.), an important component of the climate system. It is found that the critical dry diameter of CCN activity actually decreases with decrease in surface tension. In a recent study, Sareen *et al.* demonstrated that surfactants (VOCs such as methyl glyoxal and acetaldehyde) actually promote cloud droplet formation[4]. Liyana-Arachi et al. have done molecular dynamics simulations [5] of the adsorption of MS on an atmospheric air/water interface, showing that MS prefers to remain at the interface. While such observation can be rationalized by considering the hydrophilic and hydrophobic parts of MS, quantitative knowledge of the preferential binding between water and different sites of MS is essential for a full understanding of SOA formation in atmospheric aqueous phases.

MS has also been subjected to intensive spectroscopic studies since the observation of the dual fluorescence of MS by Weller in the 50s.[6,7] Weller proposed that a double potential well exists in the excited state where the ketoB* isomer gives rise to the UV band around 360 nm and the enol isomer generates the blue fluorescence at 440 nm (Figure 3.1). This photophysical scheme is the foundation of what is known as “excited state intramolecular

proton transfer" (ESIPT).[8] A great deal of experimental work in the 70s, 80s, and 90s carried out in solution, with room temperature vapor, and also in supersonic jet expansions showed that there is no equilibrium between the proposed isomers in the excited state and the related theoretical work using TDDTF and RI-CC2 calculations [9] indicated the barrier between the two proposed excited state species is so small that the conversion process is essentially barrierless.[10-14] The real-time proton transfer dynamics in the excited state from ketoB* to enol was probed by Zewail and co-workers using a femtosecond depletion technique and also by other studies.[15] Since the 1990s, the general consensus is that the dual fluorescence is due to the presence of two ground state intramolecular hydrogen (H)-bonded rotamers, ketoA and ketoB (Figure 3.2.). While ketoB is responsible for the blue band, ketoA gives rise to the UV band. More details about the fluorescence of MS in inert media and the co-existence of ketoA and ketoB conformers in the ground state were summarized by Catalán in 2012.[16]

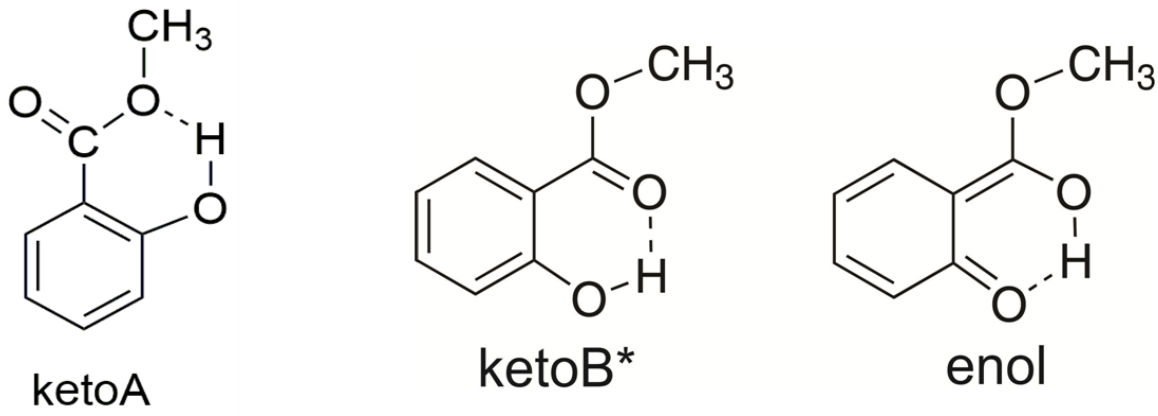

Figure 3.1 The proposed ketoA, ketoB* and enol forms of MS.

There is, however, scant direct spectroscopic evidence to support the existence of ketoA in the ground state. [11] Some earlier evidences include weak vibrational features present in thin-film IR spectra of MS at room temperature which were interpreted as due to ketoA [17] and the temperature-dependent high-resolution emission spectra of jet cooled MS which was utilized to estimate the abundance of ketoA (~1/70) at room temperature. Pimentel and co-workers[18] found only keotB isomer in the ground state in their IR matrix-isolation study, although they were able to detect ketoA as a photolysis product after irradiating the matrix with a 325 nm laser. The free-jet millimeter-wave spectroscopic study of MS by Melandri *et al.* found also only ketoB, while ketoA was calculated to be 10.04 kJ/mol less stable than

ketoB.[19] Calculations were done by using both B3LYP and MP2 methods. In 2011, Massaro *et al.*[20] reported a new theoretical investigation using the TDDFT method, in which they suggested that the ESIPT process is temperature-dependent and used this to account for the fluorescence intensity change with temperature seen in previous experiments. They further showed that the ketoA structure is not stable in the electronically excited state. In addition, the calculated conversion barrier between ketoA and ketoB was reported to be as high as 63 kJ/mol from DFT calculation and therefore chemical equilibrium between the two isomers does not occur at room temperature and the authors concluded that only ketoB exists in the ground state.[21] The above discussions underscore the need of direct evidence for the existence of ketoA.

An exciting new development in the MS saga was reported by Zhou *et al.* in 2015.[22] By noticing that the dual fluorescence of MS was observed in some aprotic solvents, such as methanol and water, and not in nonpolar solvents, such as cyclohexane,[7,9,23] these authors proposed a new mechanism where MS-solvent intermolecular H-bonding interaction plays a key role. They proposed that two different H-bonded conformers of the ketoB-solvent rather than ketoB and ketoA are responsible for the dual fluorescence behavior in aprotic solvents. Based on their calculations, the authors showed that Conf_I (Figure 3.2) where the carbonyl O of MS serves as the intermolecular H-bond acceptor precludes ESIPT and generates the near UV band, whereas Conf_II (Figure 3.2) where hydroxyl O of MS acts as the intermolecular H-bond acceptor facilitates ESIPT and gives rise to the blue band. One key question yet to be answered experimentally is the existence and the relative abundance of these two proposed intermolecular H-bonded conformers.

3.2 Previous study

Previously, the microwave spectrum of methyl salicylate and its cluster with water was studied by Mitsuzuka *et al.*[24] They have used fluorescence-detected infrared spectroscopy (FDIRS) in combination with a supersonic jet to measure IR spectra of different clusters of MS. They have studied MS clusters such as MS-$(H_2O)_n$ (n=1 and 2), MS-NH_3 and MS-CH_3OH. By scanning an IR laser frequency for a fixed value of UV laser wavelength, infrared absorption spectra of the OH stretching mode for different clusters were measured. For the MS-H_2O cluster they optimised the structure by using HF-SCF/6-31G(d,p) method. Optimisation gave two structures, which differ in their hydrogen bonding topology, i.e.

conf_I and conf_II. Their experimental results showed only the existence of the Conf_I type binding topology for both the MS-methanol and MS-H_2O complexes. In their paper they have also shown that the barrier height for the excited state *intra*molecular proton energy transfer reaction between KetoB* and the enol form depends on the solvent polarity.

One key question yet to be answered experimentally is the existence and the relative abundance of the other H-bonded conformer.

3.3 Theoretical Calculation

Substantial theoretical work for the possible conformers of MS has been reported before and only ketoA and ketoB were expected to have some population at room temperature.[18,21] We re-optimized these two structures at the MP2/6-311++G(2d,p) level. The optimized structure of KetoA and KetoB are given in Figure 3.2. For the MS-water complex, all possible geometries with water serving as an H-bond donor to the three O atoms and the aromatic ring of MS and with both ketoA and ketoB monomeric structures were considered. Calculations are done by using MP2 level of theory with 6-311++G(2d,p) basis set. We have chosen this theory due to its proven efficiency for the similar kinds of H-bonded system. Six MS-water conformers were identified and their true minimum nature was confirmed by harmonic frequency calculations. The structures of the six MS-water conformers are shown in Figure 3.2. No H-bonded MS-water conformer was found with the aromatic ring serving as the H-acceptor. In all of the monohydrate structures, the *intra*molecular H-bond is retained. Our attempt to insert water into the existing *intra*molecular H-bonded ring resulted in Conf_III, a much less stable conformation. This is in contrast to the methyl lactate-water complex [25] and a few similar systems where the insertion binding topology is the most favorable one. Apparently, the rigidity of the aromatic ring prevents the C=O and C-OH bonds from twisting in order to provide room for the insertion of a water molecule into the existing intra-molecular H-bonded ring.

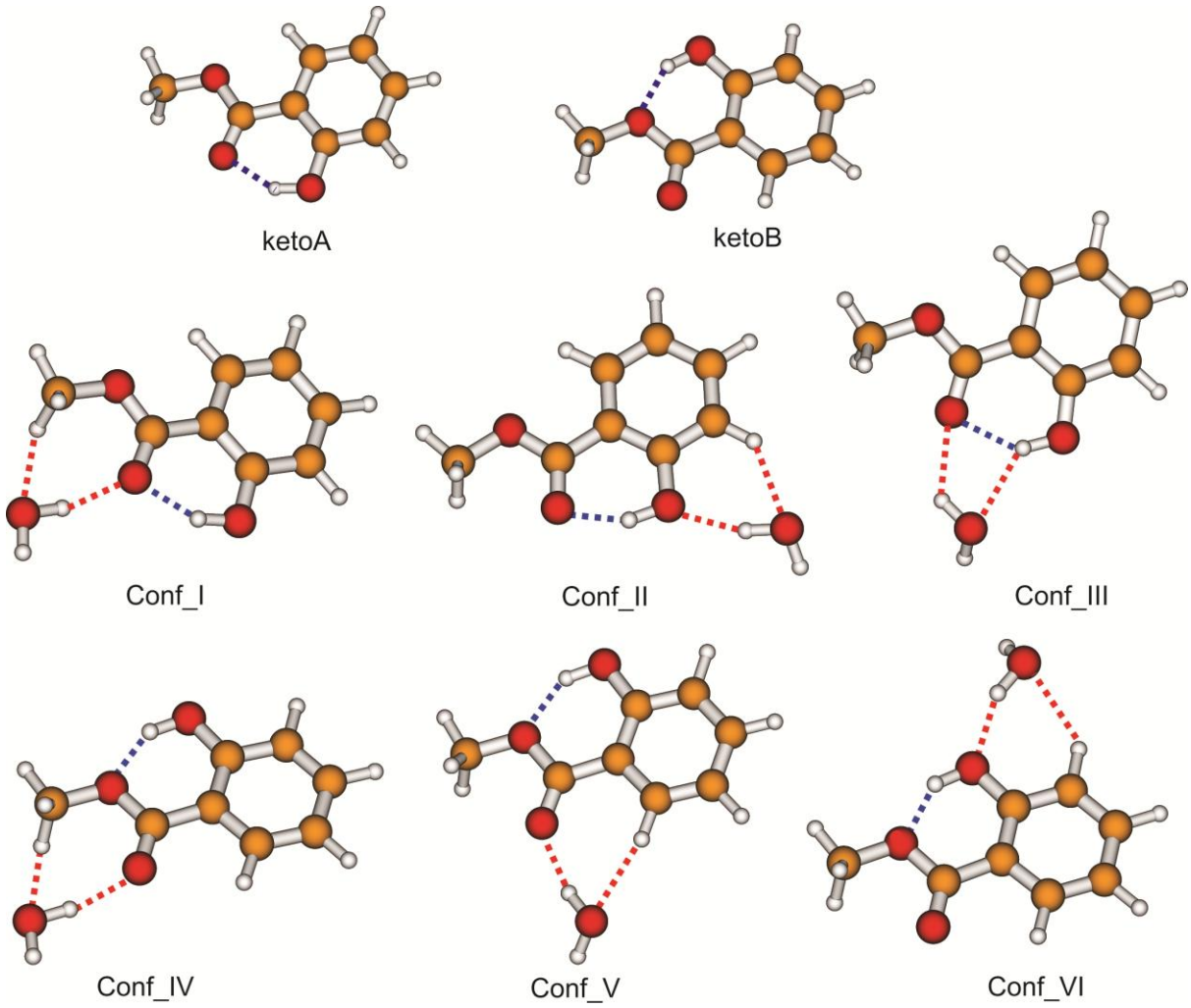

Figure 3.2 Optimized geometries of ketoA and ketoB and their six conformers of the MS-water complex at the MP2/6-311g++(2d,p) level. Important *intra*- and *inter*molecular distances are indicated with blue and red dashed lines, respectively. See text for further discussions on whether the interactions involved can be classified as the *intra*- and *inter*molecular H-bond using the bond critical point analysis.

3.4 Experimental

Experiments were carried out using the chirped pulsed and the cavity based FTMW spectrometers. Details about the spectrometers were already discussed in Chapter 2. A methyl salicylate sample obtained from Fisher Scientific (≥99 % purity) was used without further purification. As the vapour pressure of methyl salicylate is low at normal temperature, the sample had to be heated. A stainless steel sample reservoir mounted right behind a General Valve nozzle was heated to about 45 to 70 °C while the nozzle was kept at a temperature of 85 °C for the complex and 95 °C for MS itself. A schematic diagram of the set up in the chirped pulse instrument is given in Figure 3.3. As the diagram shows, in this setup the molecular beam is perpendicular to the propagation direction of the microwave excitation

radiation. For MS-water, we have used 0.05% water in 3-4 bar He as backing gas for the chirped measurements.

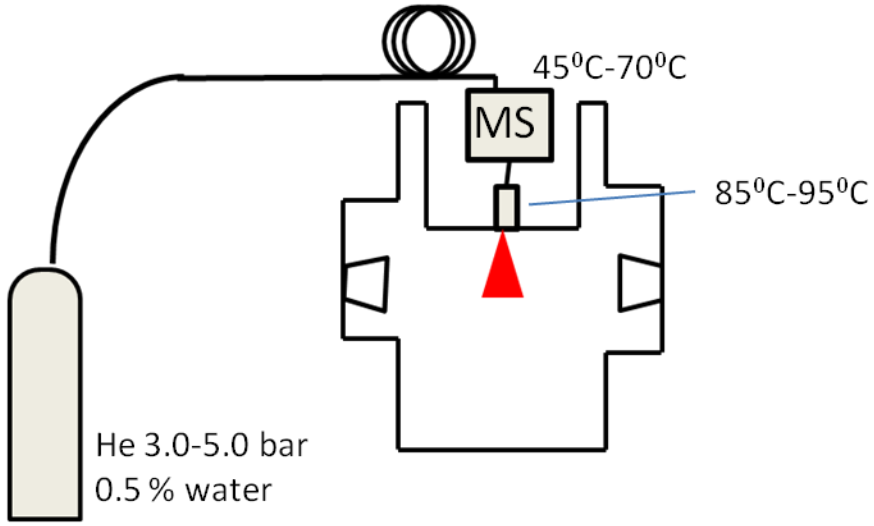

Figure 3.3 Schematic diagram of the Chirped Pulse FTMW Spectrometer with the sample system.

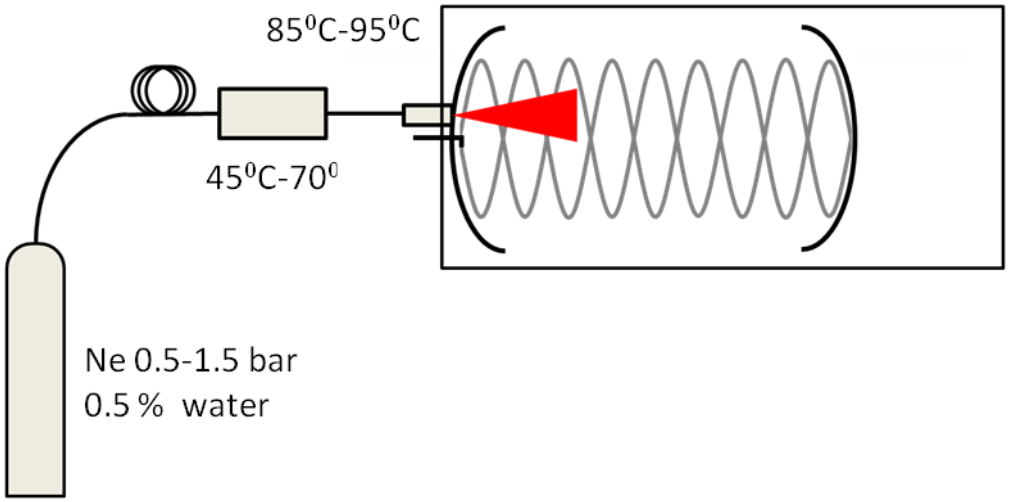

Figure 3.4 Schematic diagram of the Chirped Pulse FTMW Spectrometer with the sample system.

In case of cavity instrument I used similar temperature ranges. 0.5 to 1.5 bar of Ne was used as backing gas in cavity instrument experiments, because it results in greater signal intensity. A schematic diagram of the instrument is given in Figure 3.4. As the diagram shows, in this setup the molecular beam is parallel to the microwave propagation direction.

3.5 Results and Discussion

The results of Gaussian calculation are tabulated in tables 3.1 and 3.2. The relative raw energies, zero-point-energies (ZPE), and spectroscopic constants for ketoA, ketoB, and the three most stable MS-water conformers are summarized in Table 3.1. The corresponding results for the other conformers are given in Table 3.2.

Table 3.1 Relative raw (ΔD_e) and *ZPE* corrected (ΔD_0) energies (in kJ/mol), rotational constants (in MHz), and electric dipole components (in Debye) of Keto A, Keto B and the first three most stable conformers of methyl salicylate-water at the MP2/6-311++G(2d,p) level.

Parameter	ketoB	ketoA	Conf_I	Conf_II	Conf _III
ΔD_e[a](kJ/mol)	0	13.4	0.15	0.00	8.88
ΔD_0[a](kJ/mol)	0	12.5	0.00	0.35	7.86
A (MHz)	2167.9	2258.5	1787.9	1304.9	1129.3
B (MHz)	833.3	830.3	521.8	597.5	707.6
C (MHz)	604.2	609.4	404.9	411.5	436.7
$\lvert\mu_a\rvert$ (D)	0.69	0.41	1.76	3.29	0.36
$\lvert\mu_b\rvert$ (D)	2.89	0.76	1.68	1.21	3.25
$\lvert\mu_c\rvert$ (D)	0.00	0.00	0.00	0.88	1.38

[a] For the monomer, ΔD_e and ΔD_0 are relative to ketoB. The free energy difference between the two monomeric conformers is 11.1 kJ/mol. For MS-water, the values are relative to the most stable Conf_I where $\Delta D_e(\mathrm{i}) = D_e(\mathrm{II}) - D_e(\mathrm{i})$ and $\Delta D_0(\mathrm{i}) = D_0(\mathrm{I}) - D_0(\mathrm{i})$, where i = I-III. The significant figures do not reflect the accuracy with regard to the true values. They are given to be able to assessing differences between the isomers and conformers to help in the spectroscopic assignments.

It is interesting to note that the ZPE correction actually switches the relative stability of Conf_I and Conf_II: while Conf_II is ~0.15 kJ/mol more stable than Conf_I before ZPE correction, Conf_I is ~0.35 kJ/mol more stable after the correction. Conf_III, on the other hand, is much less stable by 8.9 kJ/mol. We therefore anticipated observing only spectra of Conf_I and Conf_II in the jet expansion.

Table 3.2 Relative raw (ΔD_e) and *ZPE* corrected (ΔD_0) energies (in kJ/mol), rotational constants (in MHz), and electric dipole components (in Debye) of the next three less stable conformers of methyl salicylate-water at the MP2/6-311++G(2d,p) level.

Parameter	Conf_IV	Conf_V	Conf_VI
ΔD_e[a](KJ/mol)	11.48	13.71	15.01
ΔD_0[a](KJ/mol)	10.89	13.42	14.03
A(MHz)	1095.52	997.22	1095.52
B(MHz)	679.94	777.36	679.94
C(MHz)	421.07	438.34	421.07
$\|\mu_a\|$ (D)	1.46	-1.08	1.46
$\|\mu_b\|$ (D)	-1.44	-2.19	-1.44
$\|\mu_c\|$ (D)	-1.08	1.02	-1.08

[a] For the monomer, ΔD_e and ΔD_0 are relative to ketoB. For MS-water, they are relative to the most stable Conf_I where $\Delta D_e(i) = D_e(II) - D_e(i)$, and $\Delta D_0(i) = D_0(I) - D_0^{ZPE}(i)$, where i = IV-VI.

3.5.1 Rotational Spectra and Rotational Constants

The spectral searches for the MS-water complex were carried out using our CP-FTMW spectrometer in the 7.7-11.7 GHz range. Both Conf_I and _II were predicted to have relatively large *a*- and *b*-dipole moment components. The free MS monomer contains a methyl internal rotor with an internal rotation barrier of 5.38(2) kJ/mol.[20] The corresponding methyl internal rotational splittings can also be expected in the complex. In addition, the water subunit may undergo tunneling motion(s) to give rise to further splittings. All this may complicate the assignment since the relative magnitudes of these splittings are not known a priori. Nevertheless, two sets of *a*- and *b*-type transitions were identified and assigned to Conf_I and _II separately based on the chirped data. A section of the broadband spectrum with transitions from both Conf_I and _II are depicted in Figure 3.5.

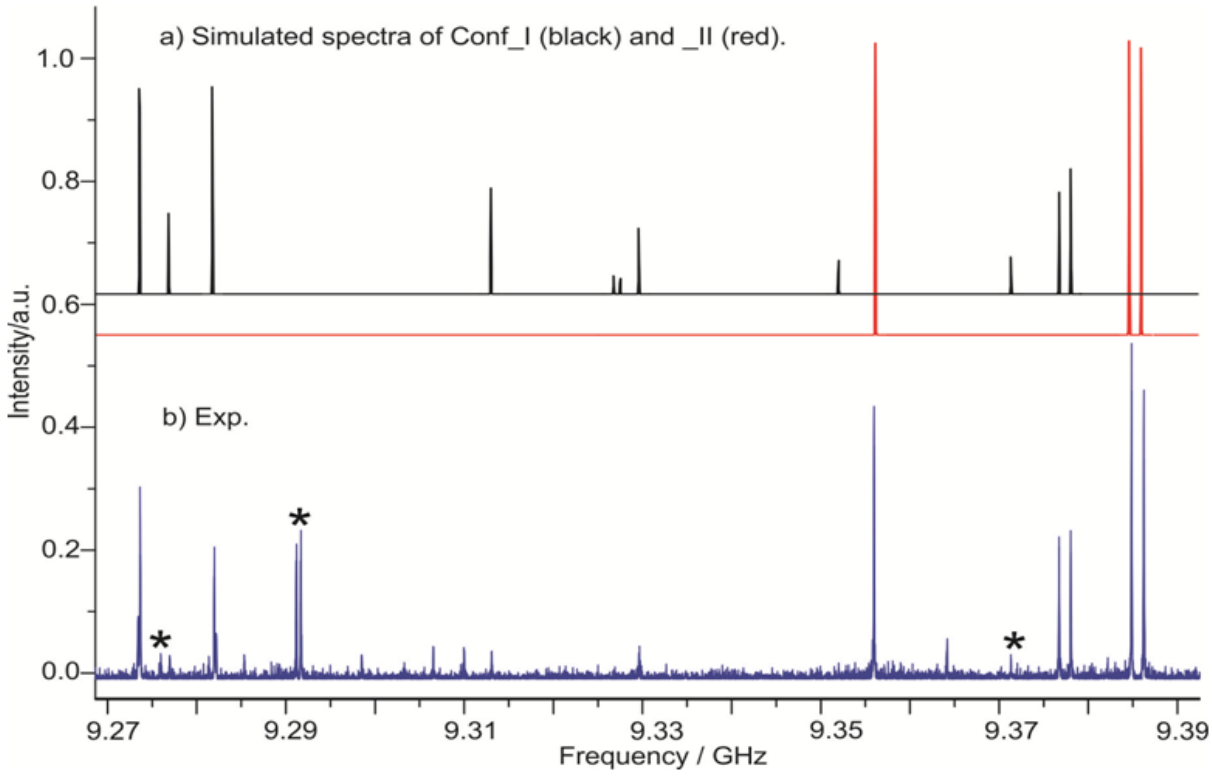

Figure 3.5 Trace a) contains simulated rotational spectra of Conf_I and II assuming a rotational temperature of 1K and the ab initio dipole moments. Trace b) is a ~0.1 GHz section of the experimental broadband spectrum recorded with MS, trace amount of water, and helium at a low backing pressure of 3 to 4 atm and 200,000 experimental cycles. * indicates transitions from the MS monomer.

The final spectral measurements were done with the cavity FTMW instrument. Small splittings on the order of tens of kHz were detected in many transitions for both Conf_I and Conf_II. Since the A/E splittings of some transitions are partially resolved and some not at all, the chirped intensity has some minor deviations from the predicted ones using a semi rigid rotor model and the calculated dipole moment components. We therefore estimated the relative abundance of Conf_I versus Conf_II based on their intensity in the 9.35-9.39 GHz region to be ~1.7. This indicates that both H-bonded conformers are of similar stability and are likely to be both in comparable abundance at room temperature in solution, supporting the newly proposed mechanism [21] for the dual fluorescence of MS in aprotic solvents.

Although the magnitudes of the small splittings observed are similar for Conf_I and _II at the first glance, it became clear through detailed spectral analyses that they are due to two different mechanisms: methyl internal rotation for Conf_I and water tunneling for Conf_II. Details about different kind of splitting are discussed in section 4.4.3. Rotational transitions

of Conf_I were fit using XIAM.[26] No *c*-type transitions could be detected, consistent with a zero *c*-type dipole component predicted. For Conf_II, transitions within the upper and lower tunneling components were fit separately with a Watson's S-reduction [27] semi-rigid rotor Hamiltonian in its I^r representation using the Pgopher program.[28] Resulting spectroscopic constants of both Conf_I and Conf_II are given in Table 3.3. All the assigned transition frequencies are provided in Table 3.4 and 3.5, respectively. The standard deviations of all the fits are about 2 or 3 kHz, similar to the measurement uncertainty of the cavity FTMW instrument.

Table 3.3 Experimental spectroscopic constants for the two MS-water conformers.

Parameter	Conf_I	Conf_II	
		Lower_comp.[a]	Upper_comp.[a]
A (MHz)	1762.78567(49)[b]	1285.8316(40)	1285.8483(44)
B (MHz)	521.66406(12)	594.73774(49)	594.73733(48)
C (MHz)	404.179054(94)	408.18396(25)	408.18587(27)
D_J (kHz)	0.01984(56)	0.0352(14)	0.0225(15)
D_{JK} (kHz)	-0.0224(40)	-0.069(16)	-0.021(19)
D_K (kHz)	0.671(33)	-0.26(17)	1.68(28)
d_1 (kHz)	-0.00568(33)	-0.0114(10)	0.00188(95)
d_2 (kHz)	-0.00090(21)	0.00044(53)	0.030(63)
V_3(kJ/mol)[c]	8.15(10)	5.83[d]	
N^e	93	35	32
σ^f (kHz)	2.3	3.4	3.7

[a] Lower and upper tunneling components due to a motion of the water subunit. See text for details. [b] Errors in parentheses are in units of the last digit. [c] Other internal parameters are: ε(rad)=3.14 and F_0=157.3 GHz, fixed at the calculated values, and δ(rad)=0.693(97). [d] Estimated from the single transition J,K_a,K_c=8,4,5-7,4,4 where the E-species was detected. [e] Number of lines fitted. [f] Standard deviation of the fit.

Table 3.4 Measured rotational transition frequencies of the most stable methyl salicylate-water conformer, Conf_I.

J'	Ka'	Kc'	J"	Ka"	Kc"	Symmetry	ν_{obs} / MHz	$\Delta\nu^a$/ kHz
6	0	6	5	0	5	A	5309.6147	0.1
6	0	6	5	0	5	E	5309.6147	0.7
6	2	5	5	2	4	A	5519.3761	-0.5
6	2	5	5	2	4	E	5519.3761	0.1
7	3	5	6	3	4	A	6527.5676	0.1
7	3	5	6	3	4	E	6527.5676	-2.2
9	1	8	8	2	7	A	6529.9454	-1.8
9	1	8	8	2	7	E	6529.9454	-4.1
7	3	4	6	3	3	A	6568.3696	-1.9
7	3	4	6	3	3	E	6568.3696	2.3
7	3	5	7	2	6	A	6745.4560	4.8
7	3	5	7	2	6	E	6745.4351	-3.9
7	1	6	6	1	5	A	6766.2024	-0.3
7	1	6	6	1	5	E	6766.2024	0.9
7	2	5	6	2	4	A	6778.5652	-0.2
7	2	5	6	2	4	E	6778.5652	1.0
8	1	8	7	1	7	A	6815.1222	-0.2
8	1	8	7	1	7	E	6815.1222	0.2
3	2	1	2	1	2	A	6892.8566	-3.4
3	2	1	2	1	2	E	6892.8566	1.4
8	3	6	8	2	7	A	6899.1092	4.9

8	3	6	8	2	7	E	6899.0882	-4.9
8	0	8	7	0	7	A	6920.5995	0.0
8	0	8	7	0	7	E	6920.5995	0.7
8	1	8	7	0	7	A	7151.1163	0.0
8	1	8	7	0	7	E	7151.1163	1.1
4	2	3	3	1	2	A	7249.4548	-6.1
4	2	3	3	1	2	E	7249.4548	0.7
8	2	7	7	2	6	A	7310.9712	1.0
8	2	7	7	2	6	E	7310.9712	1.9
8	3	6	7	3	5	A	7464.6225	-0.7
8	3	6	7	3	5	E	7464.6225	-0.9
8	4	4	7	4	3	A	7464.8424	-3.9
9	0	9	8	1	8	A	7486.5613	0.0
9	0	9	8	1	8	E	7486.5613	0.1
8	3	5	7	3	4	A	7543.7131	-1.6
8	3	5	7	3	4	E	7543.7131	0.6
9	1	9	8	1	8	A	7640.0133	0.2
9	1	9	8	1	8	E	7640.0133	0.6
8	1	7	7	1	6	A	7675.8017	0.3
8	1	7	7	1	6	E	7675.8017	1.7
9	0	9	8	0	8	A	7717.0773	-0.9
9	0	9	8	0	8	E	7717.0773	-0.3
8	2	6	7	2	5	A	7793.2333	-0.8
8	2	6	7	2	5	E	7793.2333	0.6

9	1	9	8	0	8	A	7870.5299	-0.1
9	1	9	8	0	8	E	7870.5299	0.9
5	2	4	4	1	3	A	7939.6218	-5.1
5	2	4	4	1	3	E	7939.6218	1.2
4	2	2	3	1	3	A	8070.9466	-1.3
4	2	2	3	1	3	E	8070.9466	5.0
9	2	8	8	2	7	A	8192.9695	0.7
9	2	8	8	2	7	E	8192.9695	1.8
10	1	10	9	1	9	A	8460.2994	-0.4
10	1	10	9	1	9	E	8460.2994	0.0
10	0	10	9	0	9	A	8514.0148	0.7
10	0	10	9	0	9	E	8514.0148	1.3
9	1	8	8	1	7	A	8558.7781	0.2
9	1	8	8	1	7	E	8558.7781	1.7
6	2	5	5	1	4	A	8574.5337	-2.9
6	2	5	5	1	4	E	8574.5337	3.0
10	1	10	9	0	9	A	8613.7512	-0.4
10	1	10	9	0	9	E	8613.7512	0.4
9	2	7	8	2	6	A	8799.3241	0.8
9	2	7	8	2	6	E	8799.3241	2.4
7	2	6	6	1	5	A	9159.8633	-1.3
7	2	6	6	1	5	E	9159.8633	4.3
3	3	1	2	2	0	A	9273.6729	-0.5
3	3	1	2	2	0	E	9273.3925	-1.5

11	1	11	10	1	10	A	9276.9774	-2.0
11	1	11	10	1	10	E	9276.9774	-1.5
3	3	0	2	2	1	A	9281.9613	-1.0
3	3	0	2	2	1	E	9281.9613	-0.8
11	0	11	10	0	10	A	9313.1089	-0.8
11	0	11	10	0	10	E	9313.1089	-0.2
11	1	11	10	0	10	A	9376.7176	0.7
11	1	11	10	0	10	E	9376.7176	1.4
5	2	3	4	1	4	A	9378.0281	-2.9
5	2	3	4	1	4	E	9378.0281	4.3
10	1	9	9	1	8	A	9412.8963	0.3
10	1	9	9	1	8	E	9412.8963	1.9
8	2	7	7	1	6	A	9704.6311	-1.0
8	2	7	7	1	6	E	9704.6311	4.3
4	3	2	3	2	1	A	10182.8878	0.4
4	3	2	3	2	1	E	10182.8100	-1.0
9	2	8	8	1	7	A	10221.7937	-5.8
9	2	8	8	1	7	E	10221.7937	-0.9
4	3	1	3	2	2	A	10224.7622	1.2
4	3	1	3	2	2	E	10224.8138	-2.7
5	3	3	4	2	2	A	11061.4778	-0.4
5	3	3	4	2	2	E	11061.4515	0.9
5	3	2	4	2	3	A	11187.7751	5.5
5	3	2	4	2	3	E	11187.7751	-1.0

Table 3.5 Measured rotational transition frequencies of the lower and upper components of the second most stable methyl salicylate-water conformer, Conf_II.

J'	Ka'	Kc'	J"	Ka"	Kc"	Lower Component		Upper Component	
						ν_{EXP} / MHz	$\Delta\nu^a$/ kHz	ν_{EXP} / MHz	$\Delta\nu^a$/ kHz
7	1	6	6	1	5	7069.2989	3.4	7069.3172	-1.1
7	3	5	6	3	4	7120.6336	4.8	7120.6505	8.0
7	4	4	6	4	3	7170.3173	-4.5	7170.3379	1.3
7	2	5	6	2	4	7621.9193	-1.9	7621.9404	-0.8
8	2	7	7	2	6	7656.3906	-3.5	7656.4091	-4.5
9	1	9	8	1	8	7750.0535	1.6	7750.0712	-0.3
9	0	9	8	0	8	7756.9511	0.9	7756.9689	-1.6
8	1	7	7	1	6	7867.8117	-4.8	7867.8412	0.5
8	4	5	7	4	4	8216.4636	-1.6	8216.4831	-1.9
9	2	8	8	2	7			8514.3836	-7.1
10	1	10	9	1	9	8567.9093	2.5	8567.9268	2.2
10	0	10	9	0	9	8571.0170	-0.5	8571.0346	-1.1
8	2	6	7	2	5	8636.8623	-0.5	8636.8858	-2.9
9	1	8	8	1	7	8647.9762	0.4	8647.9994	-0.1
8	3	5	7	3	4	8653.5896	-4.6	8653.6296	3.7
9	3	7	8	3	6	9061.7779	1.4	9061.7919	-3.7
10	2	9	9	2	8	9355.9644	1.8	9355.9831	-0.7
11	1	11	10	1	10	9384.8624	-0.5	9384.8812	3.7
11	0	11	10	0	10	9386.2315	-0.5	9386.2506	3.8
10	1	9	9	1	8	9432.1632	3.0	9432.1822	-0.5
9	4	5	8	4	4	9466.4450	6.6		
4	4	1	3	3	0	9505.4025	1.9		
9	2	7	8	2	6	9573.6267	-2.2	9573.6564	0.9
9	3	6	8	3	5	9823.9646	4.1		
10	3	8	9	3	7	9989.2989	-2.8	9989.3202	-1.3
11	2	10	10	2	9	10186.3356	3.4	10186.3528	0.3

12	1	12	11	1	11	10201.4111	-1.6	10201.4271	4.6
12	0	12	11	0	11	10202.0022	-1.8		
11	1	10	10	1	9	10226.7558	3.4	10226.7744	1.3
10	4	7	9	4	6	10284.3992	1.0	10284.4234	-4.2
10	2	8	9	2	7	10428.7850	-5.4	10428.8146	3.8
10	4	6	9	4	5			10666.8079	0.5
5	4	2	4	3	1	10503.3396	-0.8		
11	3	9	10	3	8	10887.7945	-4.8	10887.8198	2.0
13	1	13	12	1	12	11017.7902	-0.1	11017.7902	-3.4
13	0	13	12	0	12	11018.0402	-1.6	11018.0402	-5.0
12	1	11	11	1	10	11030.1290	3.7	11030.1468	3.3

$\Delta\nu = \nu_{obs.} - \nu_{calc.}$

3.5.2 Interaction and dissociation energy

We also have predicted the interaction and spectroscopic dissociation energies of both the stable conformers using our results from MP2 calculation. The counterpoise-corrected interaction energy [29] is calculated using the following equation:

$$\Delta E = E_{AB}^{\alpha\beta}(AB) - E_{AB}^{\alpha\beta}(A) - E_{AB}^{\alpha\beta}(B) \quad \ldots\ldots 3.1$$

Here, the subscript $\alpha\beta$ denotes the basis set used for the calculation of AB dimer and E denotes the energy of the species shown in the bracket. The interaction energies we obtained using the above equation are -20.13 kJ/mol and -20.25 kJ/mol for Conf_I and Conf_II respectively. Similarly, spectroscopic dissociation energy were calculated using the following equation:

$$D_0 = -\Delta E - (ZPE_{MS\text{-}wat} - ZPE_{MS} - ZPE_{wat}) \quad \ldots\ldots 3.2$$

where ZPE denotes the zero point energy of the species shown in the subscript. The dissociation energies we obtained are about 14.22 kJ/mol and 13.59 kJ/mol for Conf_I and Conf_II respectively.

3.4.3 Rotational Splitting

For most of the lines of conf_II splittings were observed. Splittings were also observed for some of the conf_I lines. Although the magnitudes of the small splittings observed are similar for Conf_I and _II at the first glance, it became clear through detailed spectral analyses that they are due to two different mechanisms: methyl internal rotation for Conf_I and water tunneling for Conf_II.

(a) Internal rotation of methyl group

For Conf_I, noticeable internal rotor splittings were detected in the high K *b*-type transitions. Two example transitions, 11,1,11-10,1,10 and 3,3,1-2,2,0, showing very different A/E splittings are given in Figure 3.6.

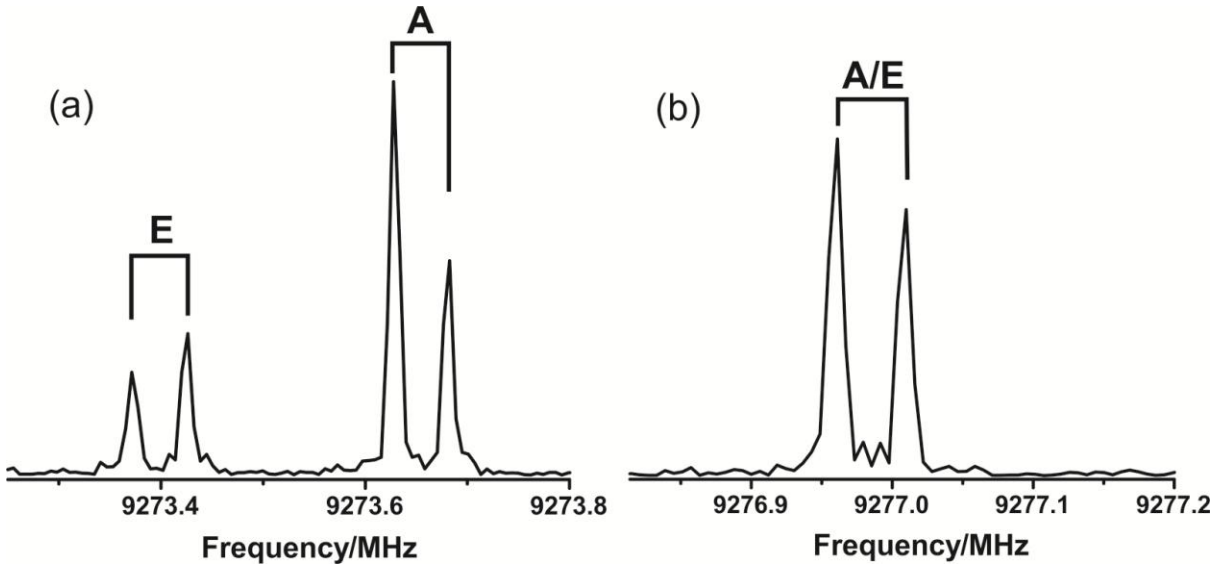

Figure 3.6 The internal rotation splitting patterns of two transitions: (a) 3,3,1-2,2,0 and (b) 11,1,11-10,1,10 of the most stable methyl salicylate-water conformer, Conf_I. For (a), the experiment was carried out at the center of E-components with 20,000 cycles.

A theoretical internal rotation barrier of 8.63 kJ/mol was calculated at the MP2/6-311++G(2d,p) level by rotating the methyl group around its C_3 axis and optimizing the rest of the structure. This value is comparably with the experimentally obtained value listed in Table 3.2. The theoretical scan is provided in Figure 3.7.

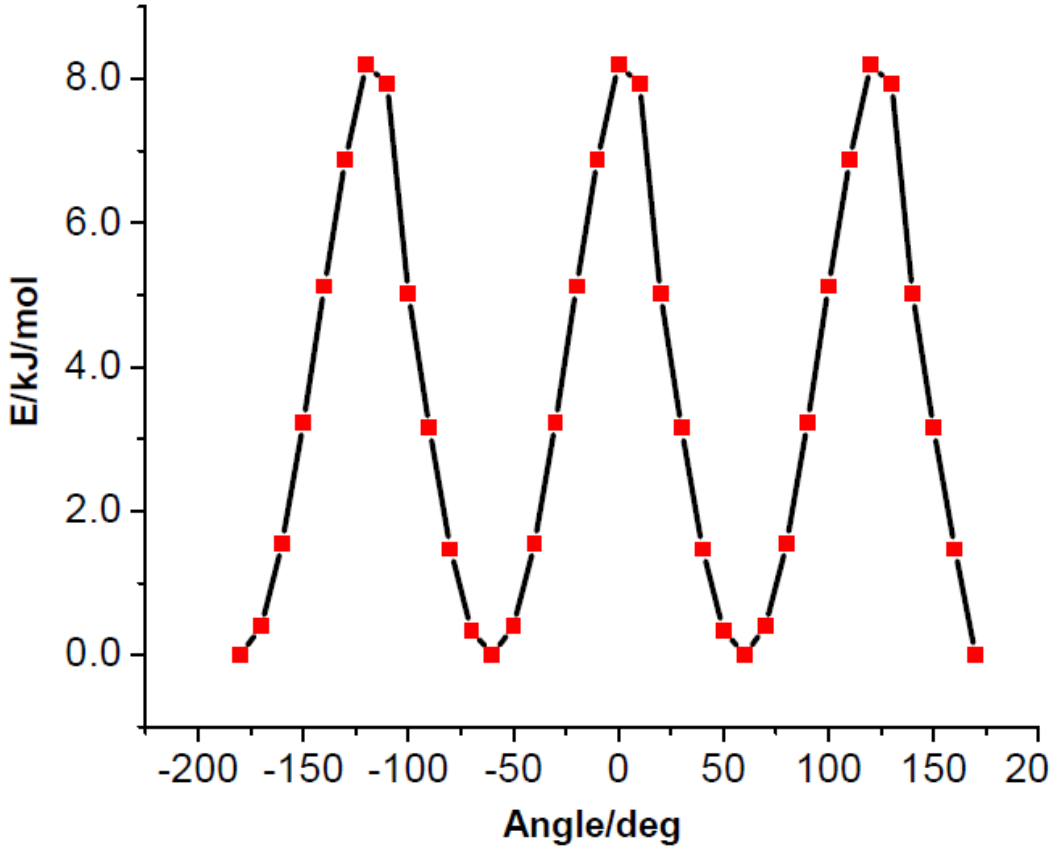

Figure 3.7 The methyl internal rotation barrier scans for the conf_I of methyl salicylate-water at the MP2/6-311++G(2d,p) level. The scans were done by rotating the methyl group around its C_3 axis and optimizing all other structural parameters.

During the methyl internal rotational scan, it was recognized that the water subunit experiences substantially movement, i.e. the methyl internal rotation is strongly coupled to the motion of the water unit. It is therefore not surprising that the barrier height of the methyl rotor in Conf_I is noticeably higher than that of the free MS. In Conf_II, on the other hand, one anticipates little interference of the water and the methyl group motions since these two units are far away from each other. Indeed, a theoretical methyl internal rotation barrier of 5.86 kJ/mol (Figure 3.8) was obtained at the MP2/6-311++G(2d,p) level, very much the same as the theoretical value of 5.88 kJ/mol obtained for the free MS and the related experimental value of 5.83 kJ/mol. One may wonder where the E-components are for Conf_II.

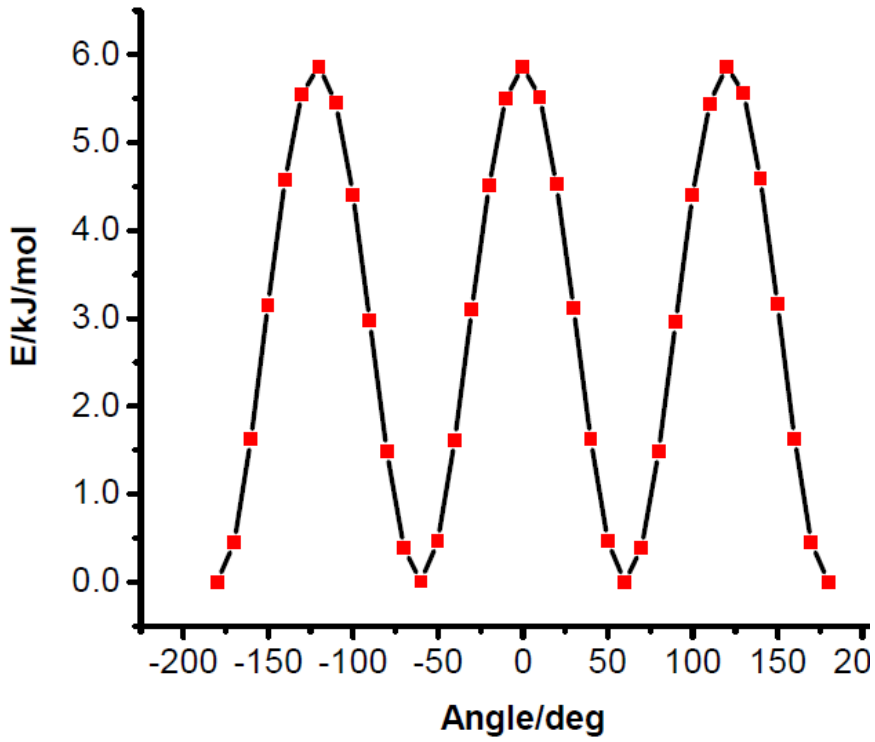

Figure 3.8 The methyl internal rotation barrier scans for the conf_II of methyl salicylate-water at the MP2/6-311++G(2d,p) level. The scans were done by rotating the methyl group around its C_3 axis and optimizing all other structural parameters.

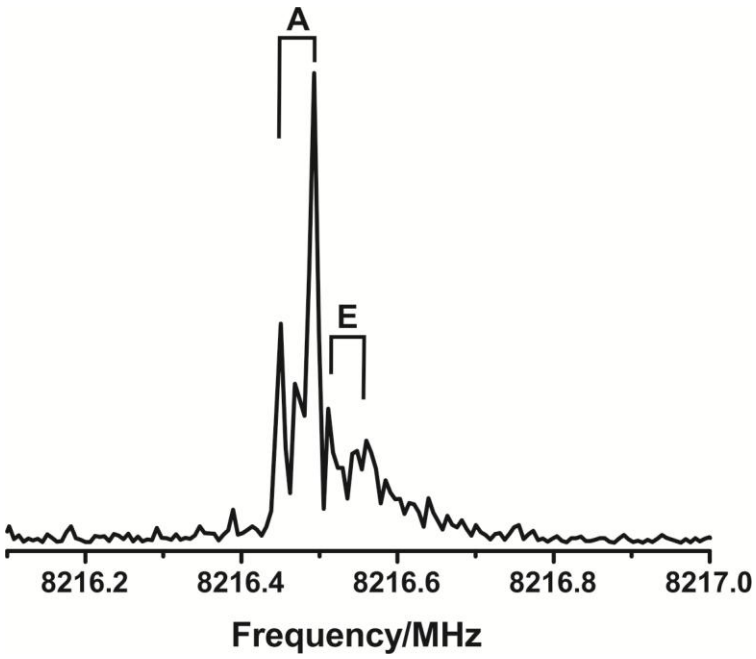

Figure 3.9 The methyl internal rotation A/E splittings of the transition, 8,4,5-7,4,4, of the second stable methyl salicylate-water conformer, Conf_II. The experiment was carried with the excitation frequency near 8216.57 MHz with 15,700 cycles. Additional narrower splittings due to the water tunneling motion are also visible.

Most transitions observed for Conf_II are low K transitions with no visible A/E splitting. It also appeared that the E-components were considerably weaker than the A-components with the additional tunneling splitting from water. To further confirm this, the E-component of 8,4,5-7,4,4 transition of Conf_II with an A/E splitting of ~66 kHz was searched and detected with 15,700 cycles (Figure 3.9). No further efforts were spent on the E-species since the signals were very weak.

(b) Water Tunneling motions

As mentioned above, most of the lines of conf_II show small splittings. One representative line of conf_II is shown in Figure 3.10. Since no other sources of splitting exist in Conf_II, aside from the methyl internal rotation discussed above, we attribute the small splitting observed to the water subunit tunneling.

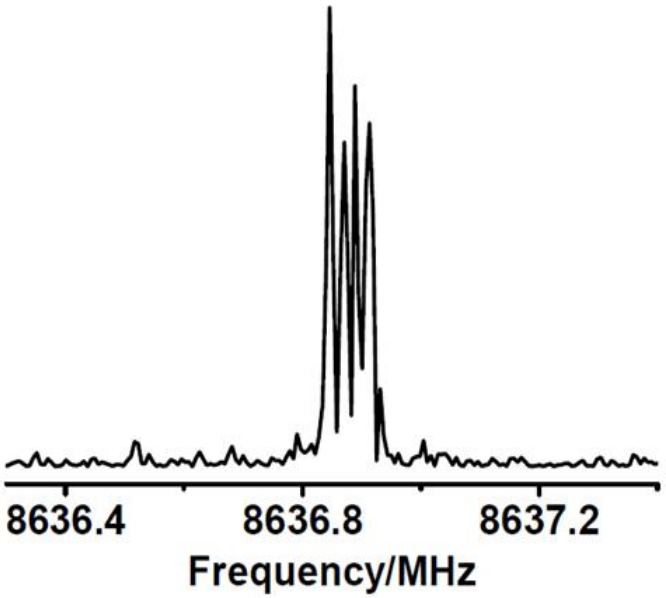

Figure 3.10 The water tunneling splittings of the transition, 8,2,6-7,2,5, of the second stable methyl salicylate-water conformer, Conf_II. The experiment was carried with the excitation frequency near 8636.85 MHz.

This assignment is confirmed by the good quality spectral fits obtained for the upper and lower tunneling components. It is interesting to examine why Conf_II exhibits H_2O tunneling splitting and Conf_I not. Such water tunneling splittings have been commonly observed in monohydrate of small molecules such as benzoic acid [30] and trifluoroanisole.[31] Since the possible tunneling motions have been discussed in detail in similar systems before, we focus on the two most plausible motions shown in Figure 3.11: (a) the rotation of the water molecule about an axis through the O atom of water and its oxygen lone pair H-bonded to the

aromatic H atom (vide infra); and Figure 3.12: (b) the wagging motion of the unbound H_w, i.e. hydrogen atom of water, from below to above the heavy-atom plane through a planar transition state. The calculated barrier for motion (a) is about 4.62 kJ/mol with both *ZPE* and *BSSE* corrections. Motion (b), on the other hand, is calculated to be barrierless (vide infra). Therefore motion (a) is likely responsible for the the observed small splttings. As discussed futher below, in motion (a), the intermolecualr H-bonding of water to the aromatic H atom is still intact. This acccounts for the lower barrier compared to a rotation about the C_2 axis of water where both H-bonds with water are broken in the transition state. For Conf_I, the corresponding motion (a) barrier was calculated to be 8.61 kJ/mol, much higher than that in Conf_II because of the intereference of the methyl group. Not suprisingly, no water tunneling splitting was detcted experimentally for Conf_I.

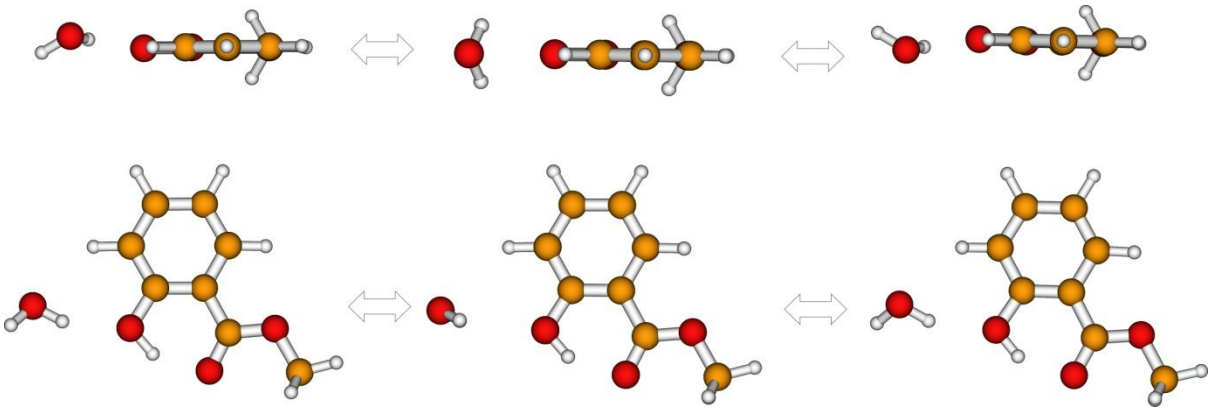

Figure 3.11 Motion (a) of the water subunit in the second most stable methyl salicylate-water complex, Conf_II: the rotation of a water molecule about an axis through the O atom and its oxygen lone pair hydrogen-bonded to the aromatic H atom.

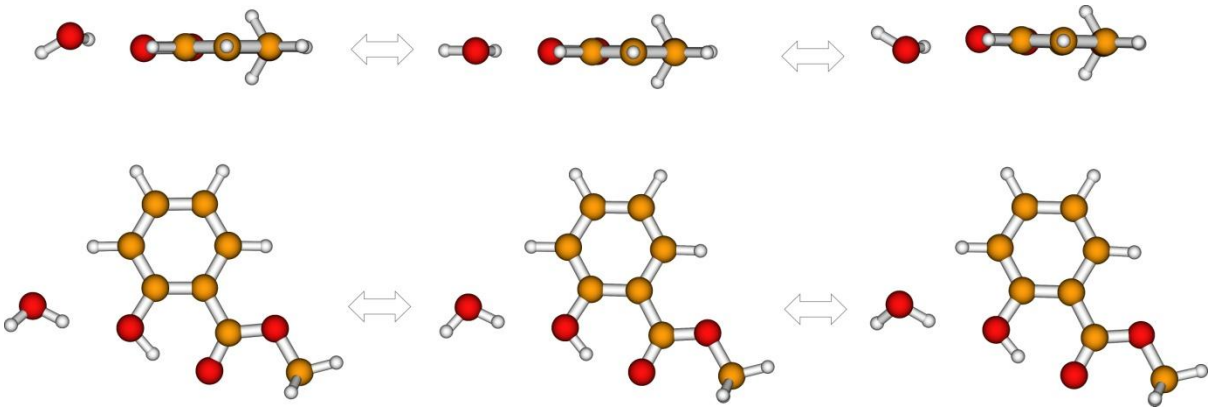

Figure 3.12 Motion (b) of the water subunit in the second most stable methyl salicylate-water complex, Conf_II: the wagging motion of the unbound H_w, i.e. hydrogen atom of water, from below to above the heavy-atom plane through a planar transition state.

It is also interesting to note that though the Conf_II has a *c*-dipole moment component of 0.9 Debye, we could not detect any *c*-type transitions. A closer examination of the structure of Conf_II suggests that this is likely due to the large amplitude wagging motion shown in Figure 3.12, which averages out the c-dipole moment. The transition state with water lying in the plane of MS was calculated to be 0.9 kJ/mol higher than the MS ketoB minimum. With the inclusion of *BSSE* and *ZPE* correction, this barrier value becomes negative at –0.67 kJ/mol. Basically, the negative value implies that the motion is barrierless and can be considered as a large amplitude motion with the unbound H_w flipping from below the MS plane to above. As a result, the average structure of Conf_II is planar with a zero *c*-dipole component, consistent with the observation. A similar observation was also reported for the benzoic acid-water complex.[30]

3.5.4 Weak Hydrogen Bonding

Conf_I and Conf_II can potentially have weak O···H-C H-bonds involving C-H as the H-bond donor, a concept of significant importance in biological systems. Detection of such a weak H-bond is generally more difficult since often a strong H-bond is also present right beside it. According to Bader's "Atoms in molecule (AIM)" theory,[32] the electron density near an atom changes upon bond formation. In particular, there is a bond critical point (BCP), i.e. the point where the gradient of the electron density vector, $\nabla\rho$, vanishes, that characterizes the formation of a chemical bond. We have performed BCP analyses for Conf_I and Conf_II using the Multiwfn program [33] and the results are summarized in Figure 3.13. The O···H-C bond distances are 2.73 and 2.46 Å for Conf_I and Conf_II, respectively, with the latter being 0.3 Å shorter than the sum of van der waals radii of the O and H atoms. Indeed, a BCP with an electron density of 0.008 a.u. was identified for this bond, falling into the typical range of an H-bond, which is from 0.002 a.u. to 0.034 a.u.[34] An estimation of the related H-bond energy, $E_{HB,}$ can be obtained from the potential energy density at a BCP with the formula: $E_{HB}= 0.5\ a_0^3\ V(r_{BCP})$ where a_0 is the Bohr radius.[35] E_{HB} for both the regular and the O···C-H H-bonds with water in Conf_II are 19.5 versus 7.4 kJ/mol, respectively, whereas in Conf_I, no BCP is identified for the O···H-C *inter*molecular contact and E_{HB} for the regular H-bond between MS and water is 19.2 kJ/mol.

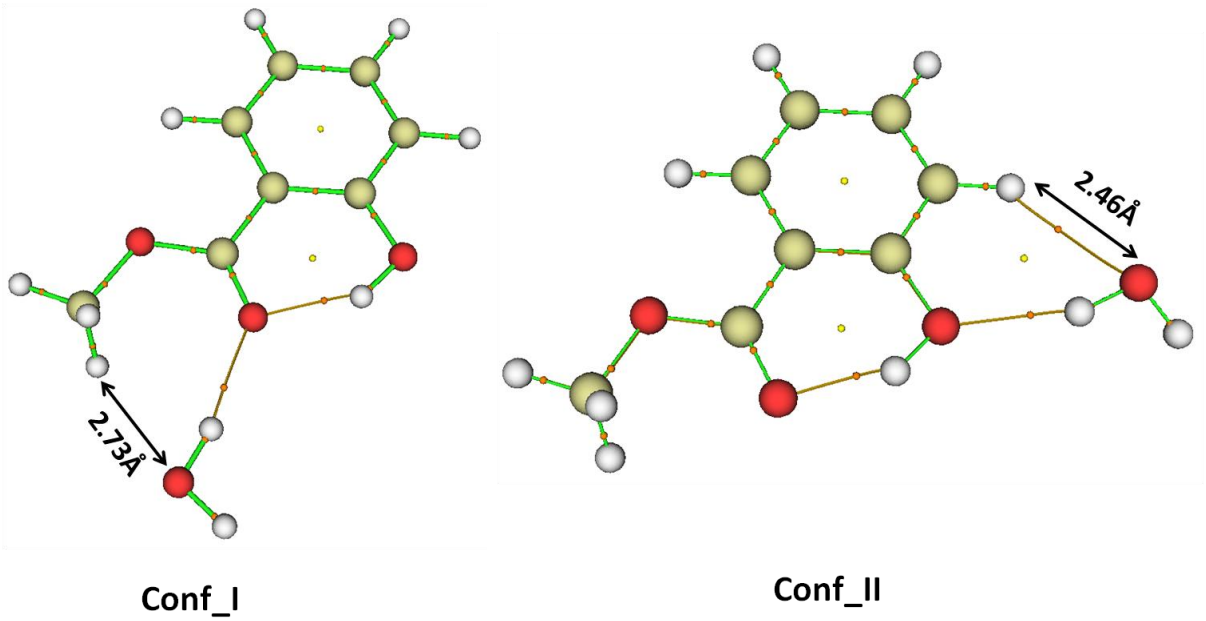

Figure 3.13 Bond crital points and ring critical points of MS-H_2O clusters. The QTAIM calculations are based on MP2 results. Orange and yellow dots denote BCPs and ring critical points, respectively. Two *inter*molecualr distances Conf_I and _II are indicated with black lines with arrows. See the text for the BCP discussions. Orange lines show the bond paths in Conf_I and _II.

3.5.5 Absence of Keto A

To search for the elusive ketoA, we first examined the ^{13}C isotopologues of ketoB. The previous temperature-dependent emission spectroscopic study estimated the abundance of ketoA to be ~1/70 at room temperature,[13] similar to that based on the calculated relative free energy in Table 3.1. Assuming a Boltzmann distribution, we can expect ~3.2% of ketoA at 95 °C. Since the natural abundance of ^{13}C is ~1%, we may expect to detect *b*-type (μ_b = 0.8 Debye) ketoA transitions if we can observe *b*-type (2.9 Debye) ^{13}C ketoB transitions in its natural abundance with a source temperature of 95 °C or higher. We have measured both A and E species of the seven ^{13}C ketoB isotopologues with ^{13}C substituted at position 1, 2, 3, 4, 5, 11, and 15 (see Figure 3.14).

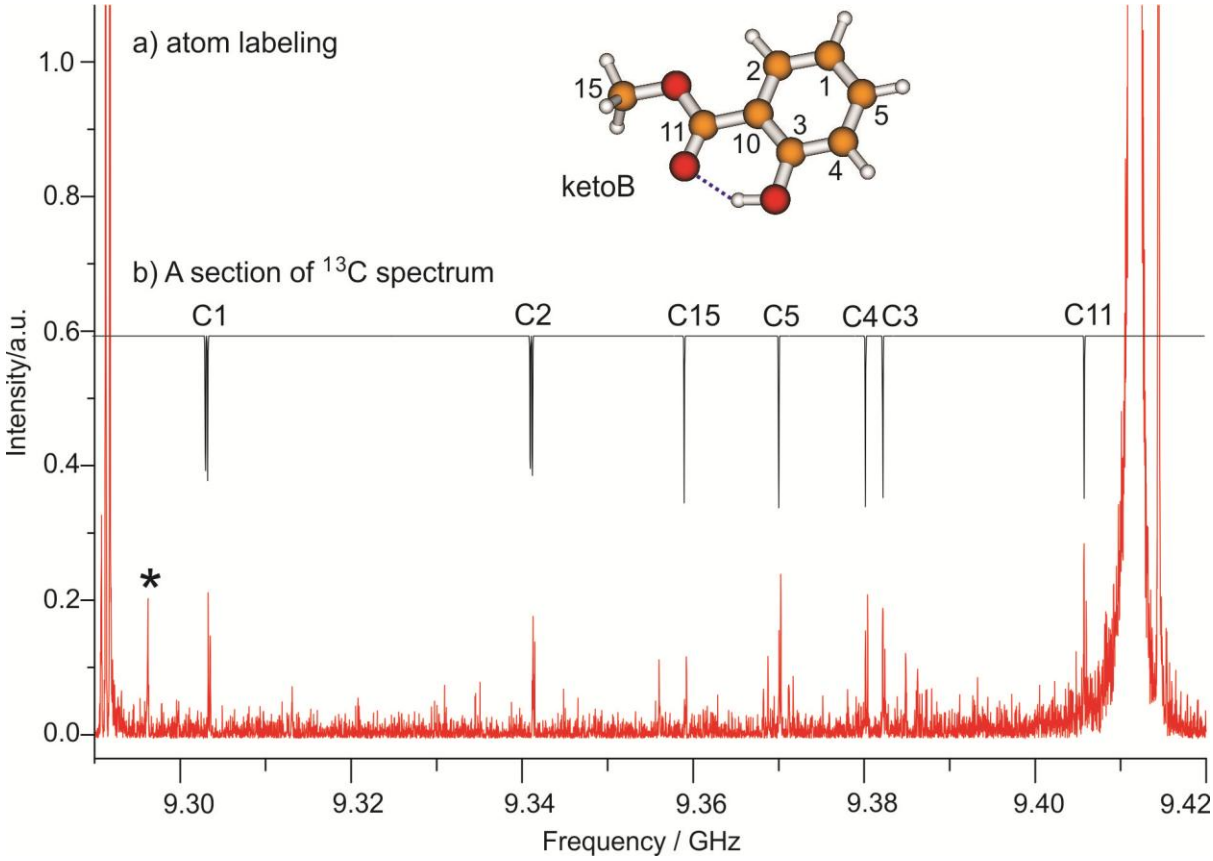

Figure 3.14 a) Carbon atom numbering; b) A section of the chirped spectrum recorded with MS in helium. The rotational transitions, 4,2,3-3,1,2, of eight ^{13}C isotopologues are indicated. The truncated strong lines at both ends of the spectrum are due to normal ketoB. Some weaker transitions are due to the assigned transitions of the MS-water complex because of the existence of trace of water in the sample system. One transition with similar intensity as ^{13}C lines, marked with *, is due to unknown impurity but not MS since this line could not be detected using the cavity FTMW spectrometer while all ^{13}C lines in the region could be detected routinely.

In fact, we have also detected the *a*-type (0.8 Debye) ^{13}C transitions easily with the cavity spectrometer. The ^{13}C substitution at position 10 is very close to the center-of-the-mass of MS and its transitions were therefore not detected due to the ^{12}C interference. The final fits were done with XIAM and the resulting constants are in Table 3.6 and 3.7, while the transition frequencies are listed in Table 3.8 and 3.9.

Table 3.6. Experimental spectroscopic constants obtained for the four ^{13}C isotopologues of the most stable methyl salicylate conformer, ketoB.

Parameter	^{13}C@1	^{13}C@2	^{13}C@3	^{13}C@4
A (MHz)[a]	2141.4128(4)	2149.1490(5)	2161.8220(3)	2165.7993(5)
B (MHz)[a]	827.2209(2)	832.0385(2)	830.9867(2)	824.4291(2)
C (MHz)[a]	599.2297(1)	602.3640(1)	602.8014(1)	599.6497(1)
V_3 (kJmol^{-1})	5.4217(4)	5.616(62)	5.54(11)	5.51(15)
P	-0.0132[b]	-0.0127(1)	-0.0134(1)	-0.0133(2)
β (rad)	3.049[b]	3.049[b]	3.108(67)	3.071(41)
γ (rad)	2.916[b]	2.916[b]	2.916[b]	2.916[b]
N[c]	16	14	13	13
σ (kHz)[d]	4.9	4.6	3.2	4.6

[a] D_J , D_{JK}, and D_K are fixed at the values of ^{12}C at 0.013, 0.037, and 0.133 kHz, respectively. [b] Fixed at the calculated values from the geometry. [c] Number of rotational transitions included in the fit.
[d] Standard deviation of the fit.

Table 3.7 Experimental spectroscopic constants obtained for the other three ^{13}C isotopologues of the most stable methyl salicylate conformer, ketoB.

Parameter	^{13}C@5	^{13}C@11	^{13}C@15
A (MHz)[a]	2165.0378(11)	2169.1662(4)	2165.3775(3)
B (MHz)[a]	821.2918(6)	830.3020(2)	816.2183(1)
C (MHz)[a]	597.9289(2)	603.0107(1)	595.2612(1)
V_3 (kJmol^{-1})	5.37(11)	5.5007(5)	5.4875(3)
ρ	-0.0135(2)	-0.0132[b]	-0.0132[b]
β (rad)	3.049[b]	3.049[b]	3.049[b]
γ (rad)	2.916[b]	2.916[b]	2.916[b]
N[c]	11	12	13
σ (kHz)[d]	4.9	4.6	3.2

[a] D_J , D_{JK}, and D_K are fixed at the values of ^{12}C at 0.013, 0.037, and 0.133 kHz, respectively. [b] Fixed at the calculated values from the geometry. [c] Number of rotational transitions included in the fit.
[d] Standard deviation of the fit.

KetoA was predicted to have a pair of strong transitions, 330-221 and 331-220, around 12.0 GHz with distinctive A/E patterns. Neither the broadband chirped nor the more targeted cavity scans in the region revealed any suitable candidates. We therefore conclude that the abundance of ketoA is even lower than ^{13}C in natural abundance. Our result tends to support

the theoretical reports [19,20] that the conversion of ketoB to ketoA is prohibited by a high barrier and only ketoB exists in the ground state. The presence of the ketoA in the previous studies is likely due to a photochemical conversion, as pointed out by Pimentel and co-workers[36] who only detected ketoA as a photolysis product after irradiating the matrix with a 325 nm laser. Future FTMW investigation of MS after such light irradiation will be of great interest in this regard. For example, laser light of 325 nm can be used to irradiate the MS sample before it enters the sample cell of the FTMW spectrometer.

Table 3.8 Measured rotational transition frequencies of ^{13}C isotopologues of the most stable methyl salicylate conformer, ketoB, substituted at position 1, 2, 3, and 4.

		^{13}C@1		^{13}C@2		^{13}C@3		^{13}C@4	
J' Ka' Kc' - J" Ka" Kc"	Sym.	ν_{EXP} / MHz	$\Delta\nu^a$ / kHz	ν_{EXP} / MHz	$\Delta\nu^a$ / kHz	ν_{EXP} / MHz	$\Delta\nu^a$ / kHz	ν_{EXP} / MHz	$\Delta\nu^a$ / kHz
221 - 110	A			7049.9346	6.0	7088.3940	3.9	7097.1685	-0.7
	E					7087.2481	4.1	7095.9869	-5.0
515 - 404	A	7070.8116	-3.7	7104.2916	-1.1	7120.8129	-0.1	7099.2586	0.5
	E	7070.7565	-5.7	7104.2381	-2.2	7120.7544	-3.5	7099.2025	-0.9
606 - 515	A	7468.4593	3.8	7510.6214	-0.3	7505.7414	2.0	7452.1557	4.0
	E	7468.4770	0.3	7510.6454	3.0	7505.7638	-0.1	7452.1761	0.3
322 - 211	A	8222.0517	3.0	8254.6580	-0.1	8293.9936	-1.1	8296.4712	0.9
	E	8221.6789	7.9	8254.2784	2.2	8293.6056	-1.1	8296.0727	-3.8
707 - 616	A	8799.7636	-1.2						
	E	8799.7806	6.6						
321 - 212	A	9039.3870	9.5	9078.6394	8.8	9110.6452	-1.5	9098.3365	8.3
	E	9039.4055	9.1	9078.6545	-4.0	9110.6749	7.0		
707 - 606	A			9085.3080	3.0				
	E			9085.2889	1.4				
624 - 523	A	9129.0042	-3.2						
	E								
717 - 606	A	9175.5446	-3.7	9221.3463	-0.2	9235.1614	-1.5	9196.8592	-1.1
	E	9175.5141	-0.1	9221.3235	10.5	9235.1320	5.4	9196.8300	5.8
423 - 312	A	9303.4310	4.6	9341.4288	-1.5	9382.4373	-0.2	9380.3930	-6.0
	E	9303.1775	-0.6	9341.1765	-5.7	9382.1800	-2.4	9380.1360	-7.0
808 - 717	A	10079.5271	4.0						
	E	10079.5271	5.0						
818 - 707	A	10292.3915	2.1						
	E	10292.3644	-0.4						

725 - 624	A	10710.8252	-3.1	10772.5330	-3.9	10761.2028	-0.2	10679.1614	-0.5
	E	10710.8252	2.0	10772.5330	1.6	10761.2028	0.0	10679.1614	2.2
331 - 220	A	11409.3820	-4.7	11451.8988	-3.9	11515.2246	0.7	11530.6581	0.3
	E	11401.5523	-3.8	11443.8930	3.4	11507.2715	-2.1	11522.6327	5.8
330 - 221	A	11438.5910	-2.5	11481.4699	-3.2	11544.1214	-1.0	11558.4917	-2.8
	E	11445.8165	-3.9	11488.8940	3.5	11551.4516	-1.6	11565.9154	4.6
817 - 716	A	11573.0644	-1.8	11633.9944	-3.0	11640.6573	1.3	11577.1216	1.8
	E	11573.0297	0.9	11633.9571	-3.1	11640.6231	2.5	11577.0858	1.2
726 - 615	A	11961.6049	-0.9	12012.3540	-0.6	12059.3246	-1.9	12048.8094	1.1
	E	11961.4219	-3.1	12012.1710	-5.0	12059.1389	-0.2	12048.6208	-1.6
826 - 725	A	12249.7522	-9.6	12319.3666	-9.6	12309.5312	-4.8	12219.7635	-7.7
	E	12249.7522	0.8	12319.3666	1.0	12309.5312	0.2	12219.7635	-0.6

[a] $\Delta\nu = \nu_{EXP} - \nu_{OBS}$

Table 3.9 Measured rotational transition frequencies of ^{13}C isotopologues of the most stable methyl salicylate conformer, ketoB, substituted at position 5, 11, and 15.

		^{13}C@		^{13}C@5		^{13}C@15	
J' Ka' Kc' - J" Ka" Kc"	Sym.	ν_{EXP} / MHz	$\Delta\nu^a$ / kHz	ν_{EXP} / MHz	$\Delta\nu^a$ /kHz	ν_{EXP} /MHz	$\Delta\nu^a$ / kHz
221 – 110	A	7093.1640	-1.4			7091.5141	1.0
	E					7090.3105	-2.5
515 – 404	A	7084.4942	-2.1	7130.0509	-0.3	7063.2102	-2.1
	E	7084.4398	-1.2	7129.9955	-1.9	7063.1535	-4.8
606 – 515	A	7425.6121	-2.6	7502.1439	3.9	7382.9220	5.2
	E	7425.6280	-10.2	7502.1628	0.6	7382.9383	-1.9
322 – 211	A	8289.0161	-9.0	8316.6577	5.0	8282.0379	0.8
	E	8288.6271	1.5	8316.2660	-0.2	8281.6378	-2.6
321 – 211	A	9084.9359	9.6	9128.9580	-0.7	9067.7347	-4.7
	E	9084.9509	-4.6	9128.9840	0.2		
717 – 606	A	9174.0809	-5.7	9242.6520	-1.4	9139.8664	-1.9
	E	9174.0510	0.6	9242.6221	3.6	9139.8372	4.6
423 – 312	A	9370.2558	2.2	9405.9873	-3.5	9359.1921	1.3
	E	9369.9936	-0.8	9405.7299	-8.9	9358.9313	-4.5
725 – 624	A			10753.6367	-2.0	10575.4470	-1.4
	E			10753.6367	3.1	10575.4470	3.6
331 – 220	A	11524.5736	0.4	11551.8546	2.5	11522.6439	12.3
	E	11516.4962	-0.3			11514.5982	4.0
330 -221	A	11552.0124	-4.1	11580.3627	3.4	11549.4127	0.1

	E			11587.7164	-0.4	11556.8726	3.3
817 – 716	A	11542.9032	11.3	11643.5293	1.4	11489.3776	1.9
	E			11643.4935	2.2	11489.3416	0.6
726 – 615	A	12032.9709	4.5	12086.2244	2.2	12013.6713	2.1
	E	12032.7824	3.5	12086.0364	-3.2	12013.4844	-1.8
826 – 725	A			12302.6751	-7.5	12104.9905	-6.3
	E			12302.6751	2.4	12104.9905	2.7

[a] $\Delta\nu = \nu_{EXP} - \nu_{OBS}$

3.5 Summary

In summary we have detected two distinctively different H-bonded MS-water conformers by using CP- and cavity based FTMW spectroscopy and found them to be of comparable stability. This is in contrast to the previous FDIRS study where only Conf_I was detected. These two binding topologies are the ones hypothesized in a recent study to promote or prohibit the ESIPT process and play crucial roles in the dual fluorescence of MS in protic solvents. The current study therefore provides important experimental evidence to support the newly proposed mechanism. Interesting interplay between the methyl internal rotation and water tunneling motions has also been investigated and an unconventional O···H-C H-bond has been analyzed using the AIM theory and identified in Conf_II. Thorough searches for ketoA were conducted and our result suggests that ketoB is the only species in the ground state under the usual conditions. Further FTMW studies of MS after light radiation will be of great interest to provide further insights into the mechanism of dual fluorescence of MS.

[1] Munger, J. W.; Jacob, D. J.; Waldman, J. M.; Hoffmann, M. R. *J. Geophys. Res. C: Oceans Atmos.* **1983**, *88*, 5109−5121.

[2] Donaldson, D. J.; Valsaraj, K. T. *Environ. Sci. Technol*. **2010**, *44*, 865−873.

[3] Richards-Henderson, N. K.; Pham, A. T.; Kirk, B. B.; Anastasio, C. *Environ. Sci. Technol*. **2015**, *49*, 268−276.

[4] Sareen, N.; Schwier, A. N.; Lathem, T. L. *Proc. Natl. Acad. Sci. USA.* **2013**, *110*, 2723−2728.

[5] Liyana-Arachi, T. P.; Hansel, A. K.; Stevens, C.; Ehrenhauser, F. S.; Valsaraj, K. T.; Hung, F. R. *J. Phys. Chem.* A **2013**, *117*, 4436−4443.

[6] Weller, A. *Naturwissenschaften*. **1955**, *42*, 175−176.

[7] Weller, A. *Z. Elektrochem.* **1956**, *60*, 1144−1147.

[8] Klöpfer, W. *Adv. Photochem.* **1977**, *10*, 311−358.

[9] Aquino, A. J. A.; Lischka, H. *J. Phys. Chem. A*, **2005**, 109 (14), 3201–3208.

[10] Klöpffer, W.; Kaufmann, G. J. Lumin. **1979**, 20, 283−289.

[11] Lopez-Delgado, R.; Sylvain, L. *J. Phys. Chem.* **1981**, *85*, 763−768.

[12] Helmbrook, L.; Kenny, J. E.; Kohler, B. E.; Scott, G. W. *J. Phys. Chem.* **1983**, *87*, 280−289.

[13] Goodman, J.; Brus, L. E. *J. Am. Chem. Soc.* **1978**, *100*, 7472−7474.

[14] Catalán, J.; Palomar, J.; dePaz, J. L. G. *J. Phys. Chem. A* **1997**, *101*, 7914−7921.

[15] Felker, P. M.; Lambert, W. R.; Zewail, A. H. *J. Chem. Phys.* **1982**, *77*, 1603-1605.

[16] Catalán, J. *Phys. Chem. Chem. Phys.* **2012**, 14, 8903−8909.

[17] Toribio, F.; Catalán, J.; Amat, F.; Acuña, A. U. *J. Phys. Chem.* **1983**, *87*, 817−822.

[18] Orton, E.; Morgan, M. A.; Pimentel, G. C. *J. Phys. Chem.* **1990**, *94*, 7936−7940.

[19] Melandri, S.; Giuliano, B. M.; Maris, A.; Favero, L. B.; Ottaviani, P.; Velino, B.; Caminati, W. *J. Phys. Chem. A* **2007**, *111*, 9076−9079.

[20] Massaro, R. D.; Blaisten-Barojas, E. *J. Chem. Phys.* **2011**, *135*, 164306(1−8).

[21] Massaro, R. D.; Dai, Y.; Blaisten-Barojas, E. *J. Phys. Chem. A* **2009**, *113*, 10385−10390.

[22] Zhou, P.; Hoffmann, M. R.; Han, K.; He, G. *J. Phys. Chem. B*, **2015**, *119*, 2125–2131.

[23] Kl pffer, W.; Naundorf, G. *J. Lumin.* **1974**, *8*, 457−461.

[24] Mitsuzuka, A.; Fujii, A.; Ebata, T,; Mikami, N. *J. Phys. Chem. A* **1998,** *102,* 9779−9784.

[25] Thomas, J.; Sukhorukov, O.; Jäger, W.; Xu, Y. *Angew. Chem. Int.* Ed. **2014**, *53*, 1156−1159.

[26] Hartwig, H.; Dreizler, H. *Z. Naturforsch*. **1996**, *51*, 923-932.

[27] Watson, J. K. G. Vol. 6 (Ed.: J. R. Durig), Elsevier, New York, **1977**, pp. 1 – 89.

[28] PGOPHER, a Program for Simulating Rotational structure, Western, C. M. University of Bristol, http://Pgopher.chm.bris.ac.uk.
[29] Boys, S. F.; Bernardi, F. Errors. *Mol. Phys*. **1970**, *19*, 553−566.

[30] Schnitzler E. G.; Jäger, W. *Phys. Chem.Chem. Phys.,* **2014**, *16*, 2305−2314.

[31 Gou, .; Spada, .; alle o- p ez, M.; Kang, L.; Novick, S. E.; Caminati, W. *J. Phys. Chem. A*, **2014**, *118*, 1047−1051.

[32] Bader, R. F. W. *J. Phys. Chem. A* **1998**, *102*, 7314−7323.

[33] Lu, T.; Chen, F. *J. Comput. Chem.* **2012**, 33, 580-592.

[34] Hobza, P. *Chem. Rev*. **2000**, 100, 4253−4264.

[35] Espinosa, E.; Molins, E.; Lecomte, C. *Chem. Phys. Lett.* **1998**, 285, 170−173.

[36] Orton, E.; Morgan, M. A.; Pimentel, G. C. *J. Phys. Chem.* **1990**, *94*, 7936−7940.

Chapter 4

Conclusions and Future Directions

The importance of *inter*molecular interactions, especially hydrogen bonding, is discussed in this thesis. Different types of H-bonding, both strong and weak, conventional and unconventional, are also discussed and it is shown how these kinds of H-bonding are important for different bio-molecules, such as nucleic acids and amino acids and other systems. Details about the theoretical modelling of H- bonds are summarised. For the current study I have used methyl salicylate as a prototype molecule. The importance of this molecule in different fields such as medical sciences, biology, environment, and spectroscopy is amply documented.

A brief description of two different kinds of FTMW spectrometers is provided. It is shown that microwave spectroscopy together with ab initio calculations is a powerful combination to study structures and dynamics of conformers of bio-molecules and their clusters with water, for example.

Finally a detailed study of methyl salicylate – water dimers is described. A number of different conformers of methyl salicylate – water dimers were identified using ab initio quantum calculations. Rotational transitions of two of these conformers were detected by chirped pulse and cavity based FTMW spectroscopy. The detection of these two conformers provides experimental support of a newly proposed mechanism for the dual fluorescence behaviour of methyl salicylate in polar solvents. The absence of the KetoA structure of the MS monomer further confirms that two different conformers of the MS – water dimers, rather than the two monomer structures, are responsible for the dual fluorescence spectrum. Different kinds of water tunnelling motions within the MS – water dimers are also discussed and it is shown how a water large amplitude motion results in an average planar structure with a zero c-dipole component, whereas a different water tunnelling motion leads to the observed splitting of the rotational lines. The internal rotation of the methyl group for both of the MS – water dimer conformers is also discussed. Topology analyses using QTAIM gives evidence for an interesting weak, unconventional H bonding involving C-H as H bond donor.

Further FTMW studies of MS after light irradiation may provide evidence for the existence of the KetoB conformer. Its detection will provide further insights into the mechanism of dual fluorescence of MS.[1,2]

Studies of other dimers with MS, for example MS-NH_3 and MS-methanol, can also be done to determine their hydrogen bonding topologies and to possibly detect several conformers. Mitsuzuka *et al.* have shown that the infrared spectral features of the MS-NH_3 complex are

different from those of MS-H_2O.[3] According to that study, in the MS-NH_3 conformer MS actually donates a proton to ammonia. The structure of MS-NH_3 is thus similar to that of Conf_III of MS-H_2O.

The signal strengths of the MS-H_2O dimer lines indicate that it may be possible to detect rotational transitions of larger clusters of the type MS-$(H_2O)_n$. It will be interesting to see into which positions the second and third water molecules will move and which additional H-bonds will be utilized to stabilize the clusters. Based on the structure of MS-H_2O, several options are possible for MS $(H_2O)_2$. For example, H_2O can bind to the water of Conf_I and Conf_II or it can bind to the other oxygen atom. Of particular interest will be if the dimer substructures (Conf_I and Conf_II) will persist in the larger clusters.

---

[1] Marsh, J. K. *J.Chem.Soc*. **1924**, 125, 418.

[2] Klopffer, W.; Kaufmann, G. *J. Lumin.* **1979**, 20, 283-289.

[3] Mitsuzuka, A.; Fujii, A.; Ebata, T,; Mikami, N. *J. Phys. Chem. A* **1998,** *102,* 9779−9784.

Bibliography

Alkorta, I.; Rozas, I.; Elguero, *J. Chem. Soc. Rev*. **1998**, 27, 163-170.

Bader, R. F. W. *Can. J. Chem.* **1964**, 42, 1822-1834.

Bader, R. F. W. *J. Phys. Chem. A* **1998**, 102, 7314−7323.

Balle, J.; Flygare, W. H. *Rev. Sci. Instrum*. **1981**, 52, 33 – 45.

Berglund, B.; Vaugham, R.W. *J. Chem. Phys.* **1980**, 73, 2037-2043.

Bernath, P.F. Spectra of Atoms and Molecules, Oxford University Press, 1995.

Bessis G.; Bratoz, S. *J. Chim. Phys.* **1960**, 57, 769.; Bessis, G. *Can. Phys.* **1961**, 127, 105.

Boys, S. F.; Bernardi, F. Errors. *Mol. Phys*. **1970**, 19, 553−566.

Brown, G. G.; Dian, B. C.; Douglass, K. O.; Geyer, S. M.; Pate, B. H. *J. Mol. Spectrosc*. **2006**, 238, 200-212.

Catalán, J. *Phys. Chem. Chem. Phys.* **2012**, 14, 8903−8909.

Catalán, J.; Palomar, J.; dePaz, J. L. G. *J. Phys. Chem. A* **1997**, 101, 7914−7921.

Coulson C. A.; Danielson, U. *Ark. Fys.***, 1955**, 8*,205*- 239.

Dempster, S.; Sukhorukov, O.; Lei, Q.-Y.; Jäger, W. *J. Chem. Phys*. **2012**, 137, 174303/1-8.

Desiraju G. R.; Steiner, T. The Weak Hydrogen Bond in Structural Chemistry and Biology (Oxford University Press, Oxford, 1999).

Donaldson, D. J.; Valsaraj, K. T. *Environ. Sci. Technol*. **2010**, *44*, 865−873.

Dyke, T.R.; Howard, B. J.; Klemperer, W. *J.Chem.Phys*. **1972**, 56, 2442.

Epstein, L. M.; Shubina, E. S.; Krylov, A. N.; Kreindlin A. Z.; Ribinskaya, M. I. *J. Organomet. Chem.,* **1993**, 447, 277-280.

Erdahl, R. M. Ph.D. Thesis, Princeton University, 1965.

Evangelisti, L.; Ecija, Cocinero, J.; Castano, F.; Lesarri, A.; Caminati, W.; Meyer, R. *J. Phys. Chem. Lett.* **2012**, 3, 3770.

Felker, P. M.; Lambert, W. R.; Zewail, A. H. *J. Chem. Phys.* **1982**, *77*, 1603-1605.

Feng, G.; Gou, Q.; Evangelisti, L.; Xia, Z.; Caminati,W. *Phys. Chem. Chem. Phys.,* **2013,** 15, 2917.

Fersht, W. H. A. Structure and Mechanism in Protein Science: A Guide to Enzyme Catalysis and Protein Folding (W. H. Freeman and Company, New York, 1999).

Gaussian 09, Rev. C.01, M. J. Frisch, G. W. Trucks, H. B. Schlegel, G. E. Scuseria, M. A. Robb, J. R. Cheeseman, G. Scalmani, V. Barone, B. Mennucci, G. A. Petersson, H. Nakatsuji, M. Caricato, X. Li, H. P. Hratchian, A. F. Izmaylov, J. Bloino, G. Zheng, J. L. Sonnenberg, M. Hada, M.Ehara, K. Toyota, R. Fukuda, J. Hasegawa, M. Ishida, T. Nakajima, Y. Honda, O. Kitao, H. Nakai, T. Vreven, J. J. A. Montgomery, J. E. Peralta, F. Ogliaro, M. Bearpark, J. J. Heyd, E. Brothers, K. N. Kudin, V. N. Staroverov, T. Keith, R. Kobayashi, J. Normand, K. Raghavachari, A. Rendell, J.C. Burant, S. S. Iyengar, J. Tomasi, M. Cossi, N. Rega, J. M. Millam, M. Klene, J. E. Knox, J. B. Cross, V. Bakken, C. Adamo, J. Jaramillo, R. Gomperts, R. E. Stratmann, O. Yazyev, A. J. Austin, R. Cammi, C. Pomelli, J. W. Ochterski, R. L. Martin, K. Morokuma, V. G. Zakrzewski, G. A.Voth, P. Salvador, J. J. Dannenberg, S. Dapprich, A. D. Daniels, O. Farkas, J. B. Foresman, J. V. Ortiz, J. Cioslowski, D. J. Fox, Gaussian, Inc.,Wallingford CT, **2010**

Goodman, J.; Brus, L. E. *J. Am. Chem. Soc.* **1978**, 100, 7472−7474.

Gou, Q.; Spada, L.; - , M.; Kang, L.; Novick, S. E.; Caminati, W. *J. Phys. Chem.* A, **2014**, 118, 1047−1051.

Grabowski, S. J. Hydrogen Bonding – New Insights (Springer, New York, 2006).

Grabowski, S. J. *Chem. Phys. Lett*. **1999**, 312, 542-547.

Grabowski, S. J. *J. Phys. Chem. A*, **2000**, 104, 5551-5557.

Hamilton W. C.; Ibers J. Hydrogen Bonding in Solids (**W.** A. Benjamin, New York, N. Y., 1968).

Hartwig, H. Dreizler, *Z. Naturforsch*. **1996**, *51a*, 923–932.

Helmbrook, L.; Kenny, J. E.; Kohler, B. E.; Scott, G. W. *J. Phys. Chem.* **1983**, *87*, 280−289.

Hofacker, L.; *Z. Naturforsch.* A*,* **1958**, 13, 1044.

Hughes, R. H.; Wilson, E. B. *Phys. Rev*. **1947**, 71 , 562-563.

Jeffrey, G. A. An Introduction to Hydrogen Bonding (Oxford University Press, New York, 1997).

Jeffrey, G. A.; Saenger, W. Hydrogen Bonding in Biology and Chemistry (Springer-Verlag, Berlin, 1991).

Kantrowitz, A.; Grey, *J. Rev*. *Sci*. *Instrum.* **1951**, 22*,* 328-332.

Klöpfer, W. *Adv. Photochem.* **1977**, 10, 311−358.

Klöpffer, W.; Kaufmann, G. *J. Lumin*. **1979**, 20, 283−289.

pffer, W.; Naundorf, G. *J. Lumin.* **1974**, 8, 457−461.

Kollman P. A.; L. C. Allen, *Chem. Rev*. **1972,** 72, 283-303.

Kvick, A.; Koetzle, T.F.; Thomas, R. *J. Chem. Phys.* **1974**, 61, 2711- 2719.

L. Paolini, *J. Chem. Phys.* **1959***,* 30, 1045.

L. Pauling, *Proc. Nat. Acad. Sci.* **1928**, 14**,** 359.

Lehninger, A. L.; Nelson, D. L.; Cox, M. M. Lehninger Principles of Biochemistry (Worth Publishers, New York, 2000).

Leszczynski, J.; *Adv. Mol. Struct. Res*. **2000**, 6, 209-265.

Liyana-Arachi, T. P.; Hansel, A. K.; Stevens, C.; Ehrenhauser, F. S.; Valsaraj, K. T.; Hung, F. R. *J. Phys. Chem.* A **2013**, 117, 4436−4443.

Lopez-Delgado, R.; Sylvain, L. *J. Phys. Chem.* **1981**, 85, 763−768.

Lu, T.; Chen, F. *J. Comput. Chem.* **2012**, 33, 580-592.

Massaro, R. D.; Blaisten-Barojas, E. *J. Chem. Phys.* **2011**, 135, 164306(1−8).

Massaro, R. D.; Dai, Y.; Blaisten-Barojas, E. *J. Phys. Chem. A* **2009**, *113*, 10385−10390.

McAfee, K. B.; Hughes, R. H.; Wilson Jr., E. B. *Rev. Sci. Instrum*. **1949**, *20*, 821-826.

McGurk, J. C.; Schmalz, T. G.; Flygare, W.H. *Density Matrix, Bloch Equation Description of Infrared and Microwave Transient Phenomena*; (eds.; In Prigogine, I.; Rice, S.A.), 1974.

Melandri, S.; Giuliano, B. M.; Maris, A.; Favero, L. B.; Ottaviani, P.; Velino, B.; Caminati, W. *J. Phys. Chem. A* **2007**, 111, 9076−9079.

Mitsuzuka, A.; Fujii, A.; Ebata, T,; Mikami, N. *J. Phys. Chem. A* **1998,** 102*,* 9779−9784.

Munger, J. W.; Jacob, D. J.; Waldman, J. M.; Hoffmann, M. R. *J. Geophys. Res. C: Oceans Atmos.* **1983**, 88, 5109−5121.

Ogasawara, H.; Brena, B.; Nordland, D.; Nyberg, M.; Pelmenschikov, A.; Petterson L. G.M.; Nilsson, A. *Phys. Rev. Lett.* **2002**, 89, 276102(1-4).

Orton, E.; Morgan, M. A.; Pimentel, G. C. *J. Phys. Chem.* **1990**, *94*, 7936−7940.

Kollman, P. A.; Allen, L. C. *J. Am. Chem. Soc.* **1970**, 92, 4108-4110.

Palusiak, M.; Grabowski, S.J. *J. Mol. Struct. Theochem*, **2004**, 674, 147-152.

Park, S-W.; Kaimoyo, E.; Kumar, D.; Mosher, S.; Klessig, D.F. Science **2007**, 318, 113-116.

Pauling, L. The Nature of the Chemical Bond (Cornell University press, Ithaka, New York, 1960).

Pgopher, a Program for Simulating Rotational Structure, C. M. Western, University of Bristol, http://Pgopher.chm.bris.ac.uk.

Pimentel G. C.; McClellan, A. L. The Hydrogen Bond (W.H Freeman, Sari Francisco Calif., 1960)

Popelier, P.L.A. *J.Phys. Chem*. A, **1998**, 102, 1873-1878.

Ramachandran, G.N.; Chandrasekharan, R. Biopolymers **1968**, 6, 1649-1658.

Richards-Henderson, N.K; Pham, A.T.; Kirk, B.B; Anastasio, C. Environ. Sci. Technol. **2015**, 49, 268-276.

Rubin, J.; Brennan, T.; Sundaralingam, M. *Biochem.* **1972**, 11, 3112- 3128.

Saenger, W. Principles of Nucleic Acid Structure (Springer-Verlag, New York, 1984).

Saenger, W. *Angew. Chem., Int. Ed. Engl.* **1973,** 12, 591-601.

Saggu, M.; Levinson N. M.; Boxer S. G. *J. Am. Chem. Soc.* **2012**, 134, 18986-18997.

Sareen, N.; Schwier, A. N.; Lathem, T. L. *Proc. Natl. Acad. Sci. USA.* **2013**, *110*, 2723−2728.

Schmalz, T. G.; Flygare, W.H. Laser and Coherence Spectroscopy, (ed.; Steinfeld, J. I.) Plenum, New York, 1978, 125–196.

Schnitzler E. G.; Jäger, W. *Phys. Chem.Chem. Phys.,* **2014**, 16, 2305−2314.

Schulz G. E.; Schirmer, R. H. Principles of Protein Structure (Springer- Verlag, New York, 1979).

Shulaev, V.; Silverman, P.; Raskin, I. *Nature* **1997,** 385, 718-721.

Sponer, J.; Leszczynski, J.; Hobza, P. *J. Phys. Chem.* **1996**, 100, 1965-1974.

Sussman, J.L.; Seeman, N.C.; Kim, S.-H.; Berman, H.M. *J. Mol. Biol*. **1972,** 66, 403-421.

Sutor, D.J. Nature **1962**, 195, 68-69.

Sutor, D.J.; *J. Chem. Soc*. **1963**, 35, 1105-1110.

Tanjaroon, C,; Jäger, W. *J. Chem. Phys,* **2007**, 127, 34302.

Thomas, J. Ph.D. Thesis, University of Alberta, 2014.

Thomas, J.; Sukhorukov, O.; Jäger, W.; Xu, Y. *Angew. Chem. Int.* Ed. **2014**, *53*, 1156−1159.

Toribio, F.; Catalán, J.; Am t, F .; Acuň , A. U. *J. Phys. Chem.* **1983**, 87, 817−822.

Townes, C.H.; Schawlow, A.L. Microwave Spectroscopy, Dover Publications, 1955.

Tsubomura, H. *Bull. Chem.Soc. Jap.* **1954**, 27,445.

Watson, J. K. G. Vol. 6 (Ed.: J. R. Durig), Elsevier, New York, **1977**, 1 – 89.

Weller, A. *Naturwissenschaften*. **1955**, 42, 175−176.

Weller, A. *Z. Elektrochem.* **1956**, 60, 1144−1147.

Wong, M. A.; Frisch, M. J.; Wiberg, K. B. *J. Am. Chem. Soc.* **1992**, 114 , 523- 529.

Xu, Y.; Jäger, W. *J. Chem. Phys*. **1997**, 106, 7968-7980.

Xu, Y.; Wijngaarden, J. van.; Jäger, W. *Int. Rev. Phys. Chem*. **2005**, 24, 301-338.

Zhou, P.; Hoffmann, M. R.; Han, K.; He, G. *J. Phys. Chem.* B, **2015**, *119*, 2125–2131.